PLANT SCIENCES

Natural variation in a cortex/epidermis-specific transcription factor bZIP89 determines lateral root development and drought resilience in maize

Pengcheng Li[1,2]*†, Tianze Zhu[1,2]†, Yunyun Wang[1,2]†, Xiaomin Zhang[3], Xiaoyi Yang[1,2], Shuai Fang[1,2], Wei Li[1,2], Wenye Rui[1,2], Aiqing Yang[1,2], Yamin Duan[1,2], Yuxing Yan[1,2], Qingchun Pan[4], Zhongtao Jia[4], Houmiao Wang[1,2], Zefeng Yang[1,2], Peng Yu[5,6]*, Chenwu Xu[1,2]*

Lateral roots (LRs) branching is crucial for water and nutrient acquisition in plants, ultimately determining the overall plant performance and productivity. However, the transcriptional regulation of LR development in crops and its role in stress resilience remain largely unexplored. Leveraging integrated transcriptome-wide association study and single-cell RNA sequencing data, we identified a basic leucine zipper (bZIP) transcription factor *ZmbZIP89* as an important regulator of LR elongation and mapped its spatial expression pattern in cortex/epidermis cell types. ZmbZIP89 can activate the expression of *ZmPRX47* to regulate the production of root reactive oxygen species homeostasis, contributing to increased lateral root length (LRL) and enhanced drought resistance. Natural variations in the 3′ untranslated region of *ZmbZIP89* enhance gene expression by increasing mRNA stability, leading to increases in LRL and drought tolerance. These findings contribute to our understanding of the molecular mechanisms underlying LR development and provide potential gene targets for breeding stress-resilient crops.

INTRODUCTION

Maize (*Zea mays* L.) is a cereal crop with a highly complex root system architecture (*1*). Moreover, its nutrient uptake (*2*, *3*) and stress resilience (*4*, *5*) are largely determined by the formation and spatial patterning of lateral roots (*6*). Root development and functions have been reshaped by domestication (*7*) and local adaptation (*8*) from natural habitats to agricultural systems. To date, several studies have provided forward (*9*, *10*) and reverse (*11*, *12*) genetic evidence of the molecular basis of root structures and functions, which are partially regulated by environmental factors, especially abiotic stresses. Nevertheless, the question of how monocot species configured the cell patterning and differentiation and to which degree the developed root architecture in adaptation to stress remain relatively unknown in cereals. This genetic and molecular information is essential to understand the potential value of root adaptation to changing environments and the subsequent development of crop cultivars resilient to future climatic challenges.

Maize has a complex root system comprising embryonic primary root, seminal roots, and post-embryonic shoot-borne roots, as well as lateral roots (*1*). Longitudinally, the primary root can be divided into three developmental zones (i.e., meristematic, elongation, and differentiation zones) (*13*). All maize root types share a common anatomical organization, including the epidermis, cortex, endodermis, and stele, which contains the pericycle, phloem, and xylem (*13*). The major cell types, including pericycle cells and endodermal cell files, are involved in the initiation and elongation of a single lateral root, ultimately shaping the root system architecture and functionality (*14*, *15*). Early pericycle cell RNA sequencing analyses revealed that plant hormones and specific transcription factors (TFs) determined the formation and function of lateral roots in maize (*2*, *16*). These genes were recently functionally characterized using reverse genetic approaches (*11*, *12*). However, unlike the model plant *Arabidopsis thaliana*, cereal crops require their primed pericycle cells and differentiated lateral root primordia to penetrate several layers of cortical cells to produce a mature lateral root (*13*, *17*). Determining which cell type and developmental process are the major determinants of root system architecture and function is challenging if the classical genetic or molecular approaches that mask the inherent heterogeneity of expression among different cell types are used. Recent advances in single-cell RNA sequencing (scRNA-seq) have revolutionized the exploration of plant root development, enabling the identification of cell type–specific genes, pathways, and regulatory networks involved in root growth and development (*17*–*20*). Several hormones, e.g., ethylene and brassinosteroid, play critical roles in influencing root development within the epidermal and cortical cell layers of *A. thaliana* (*18*, *21*). Several classical ABF2 and ABF3 TFs have been identified as nitrate-responsive functional regulators in endodermal cells (*22*). In maize, a single-cell resolution map of the root system has been constructed, revealing that the SHORT-ROOT signaling pathway regulates the number of cortex layers (*17*), thus determining the distinctive complexity of cereal root anatomy. Despite these advancements, the cell type–specific regulators and gene regulatory networks involved in root development and stress adaptations in cereals remain to be fully elucidated.

[1]Jiangsu Key Laboratory of Crop Genomics and Molecular Breeding/Key Laboratory of Plant Functional Genomics of the Ministry of Education, Agriculture College of Yangzhou University, Yangzhou 225009, China. [2]Jiangsu Co-Innovation Center for Modern Production Technology of Grain Crops/Jiangsu Key Laboratory of Crop Genetics and Physiology, Yangzhou University, Yangzhou 225009, China. [3]State Key Laboratory of Crop Stress Adaptation and Improvement, Academy for Advanced Interdisciplinary Studies, School of Life Sciences, Henan University, Kaifeng 475004, China. [4]State Key Laboratory of Nutrient Use and Management, College of Resources and Environmental Sciences, China Agricultural University, Beijing 100193, China. [5]Emmy Noether Group Root Functional Biology, Institute of Crop Science and Resource Conservation (INRES), University of Bonn, Bonn 53113, Germany. [6]Plant Genetics, TUM School of Life Sciences, Technical University of Munich, Freising 85354, Germany.
*Corresponding author. Email: pcli@yzu.edu.cn (P.L.); pengyu.yu@tum.de (P.Y.); cwxu@yzu.edu.cn (C.X.)
†These authors contributed equally to this work.

Population genetics offers a powerful framework for exploring root genetics and translating these insights into strategies for crop improvement and sustainable agriculture. We produced and integrated the transcriptome-wide association study (TWAS) data using transcriptome data of 357 maize inbred lines and the results of a scRNA-seq analysis based on the maize reference genotype B73. We identified several key regulatory genes involved in root development underlying complex quantitative traits in maize. In particular, we identified *ZmbZIP89* as a key TF affecting lateral root development and mapped its spatial expression pattern in cortex/epidermis cells. We further established a *ZmbZIP89*-mediated regulatory network, and demonstrated that ZmbZIP89 activates the expression of a peroxidase (POD) gene *ZmPRX47*, thereby facilitating reactive oxygen species (ROS) production. The ZmbZIP89-ZmPRX47-ROS module was functionally validated as a key component mediating root development and maize drought resilience. Notably, sequence variations in 3′ untranslated region (UTR) of *ZmbZIP89* provided a link between natural variation in lateral root development and gene expression levels. Our study provides valuable insights into the genetic network regulating cell-specific aspects of root development and offers valuable genomic resources for improving the root system to enhance stress resilience in maize.

RESULTS

Root phenotypic and transcriptomic analyses for a maize diversity panel

We hydroponically cultured a maize diversity panel ($n = 357$; table S1) and evaluated root phenotypic traits at the seedling stage (14-day growth period). Whole root systems were scanned and the total lateral root length (LRL) was calculated to reflect the overall absorption surface of the whole root system. There was substantial phenotypic variation for LRL within the panel, ranging from 44.9 to 836.9 cm (fig. S1). To identify genes affecting LRL, a bulk RNA-seq analysis was conducted to determine global gene expression profiles in the lateral roots of representative lines. After low-quality reads were removed, 13 billion paired-end reads were generated, with an average of 36.8 million reads for each accession (table S2). Clean reads were mapped to the Zm-B73-REFERENCE-NAM-5.0 reference genome, with an average unique read mapping rate of 84.47% (tables S2 and S3). After normalization and removal of genes with low expression levels [those genes with transcripts per million (TPM) value greater than 0.5 for at least 80% of the accessions], a total of 21,697 genes were retained for further analyses.

TWAS identified lateral root–related genes

To explore the genetic basis of root development, we performed a TWAS using the expression levels of 21,697 genes to identify causal associations between gene expression and LRL. Notably, 647 genes were significantly [false discovery rate (FDR) < 0.05] associated with LRL (Fig. 1A and table S4). These genes were functionally characterized according to a Gene Ontology (GO) enrichment analysis. The significantly enriched GO categories included cell wall organization or biogenesis (GO: 0071554), which included genes encoding expansins (*EXPA2*, *EXPA3*, *EXPB4*, and *EXPB11*), xyloglucan endotransglucosylases (*XTH6* and *XTH7*), and cellulose synthases (*CESA8*, *CESA10*, and *CSLD2*), as well as ROS metabolic process (GO: 0072593), which included genes encoding PODs and superoxide dismutase (*SOD10*) (Fig. 1B). In addition, several auxin-related genes were identified, including Aux/IAA TF (*IAA4*, *IAA10*, *IAA11*, and *IAA21*) and auxin-responsive genes (*SAUR21* and *SAUR79*). Thirty-seven TFs from 17 TF families (e.g., MYB, HD-ZIP, bZIP, NAC, and MADS) were significantly associated with LRL (Fig. 1A, fig. S2, and tables S4 and S5). We further explored the network associations between these 37 TFs and 647 potentially coregulated genes based on gene expression profiles in 357 inbred lines. A total of 9327 TF–coexpressed target gene pairs were identified in TF regulatory networks (Fig. 1C and table S6). The top nine most connected TFs were *DBB11*, *THX18, HB49*, *bZIP53*, *HB98*, *THX26*, *bZIP89*, *bHLH74*, and *EREB17*, which were involved in network associations involving more than 400 genes in each network (table S5).

Single-cell transcriptome of the maize seedling primary root

A single-cell transcriptome analysis was performed for a high-resolution examination of the cellular heterogeneity and spatial patterns of gene expression in maize primary root. Three representative regions of primary root ($n = 100$) of the reference maize genotype B73 were dissected and mixed to enzymatically generate protoplasts for a transcriptome analysis using the 10× Genomics platform (Fig. 2A). A standardized pipeline (Cell Ranger v6.0) was applied to filter the high-quality cells and high-confidence genes. Our scRNA-seq analysis detected 29,266 expressed genes in 12,190 cells, with a mean of 35,876 reads per cell and a median of 2362 genes per cell (table S7). Using the uniform manifold approximation and projection (UMAP) method, the captured cells were classified into 21 transcriptionally distinct clusters (Fig. 2B). To annotate these clusters, we used 27 cluster marker genes whose functions, and expression patterns have been well studied (tables S8 and S9 and fig. S3A). As a result, 21 distinct cell clusters were annotated into 10 cell populations: cortex (C0, C3 and C9), exodermis (C11 and C19), epidermis (C4), endodermis (C12), phloem (C8 and 1C4), stele (C5, C7, C15 and C18), xylem (C6 and C16), pericycle (C1 and C10), meristem (C13), and root cap (C17) (Fig. 2B and fig. S3A). We identified several subtypes of stele (C5, C7, C15, and C18) and cortex (C0, C3, and C9) tissues that were marked with a sequential of cell state progression by pseudotime analysis (fig. S3, B to E), thus reflecting the varying developmental status of the stele and cortical tissue differentiation along the progression of root development. Our single-cell transcriptome analysis revealed the complex cellular landscape of the developing maize root, highlighting the heterogeneity in cell type composition and developmental states within both the stele and cortex.

LRL-associated genes were mainly enriched in the epidermis and cortex

To determine the candidate genes involved in lateral root development at cellular resolution, we analyzed our scRNA-seq results for data regarding 647 genes identified by TWAS. The AUCell R package can score gene set activity for each cell based on gene set enrichment analysis in scRNA-seq data (*23*). We determined that 647 LRL-associated genes were mainly enriched in cell clusters C0 and C4, which correspond to the cortex and epidermis cell types, respectively, with additional enrichment in clusters C6 and C14 (Fig. 2C). Moreover, C0 and C4 had most LRL-associated genes among all cell clusters, with 128 and 146 genes, respectively (Fig. 2E and fig. S4). A GO analysis revealed that LRL-associated genes in C0 and C4 were significantly associated with several processes, including plant-type cell wall organization or biogenesis (GO: 0071554), POD activity

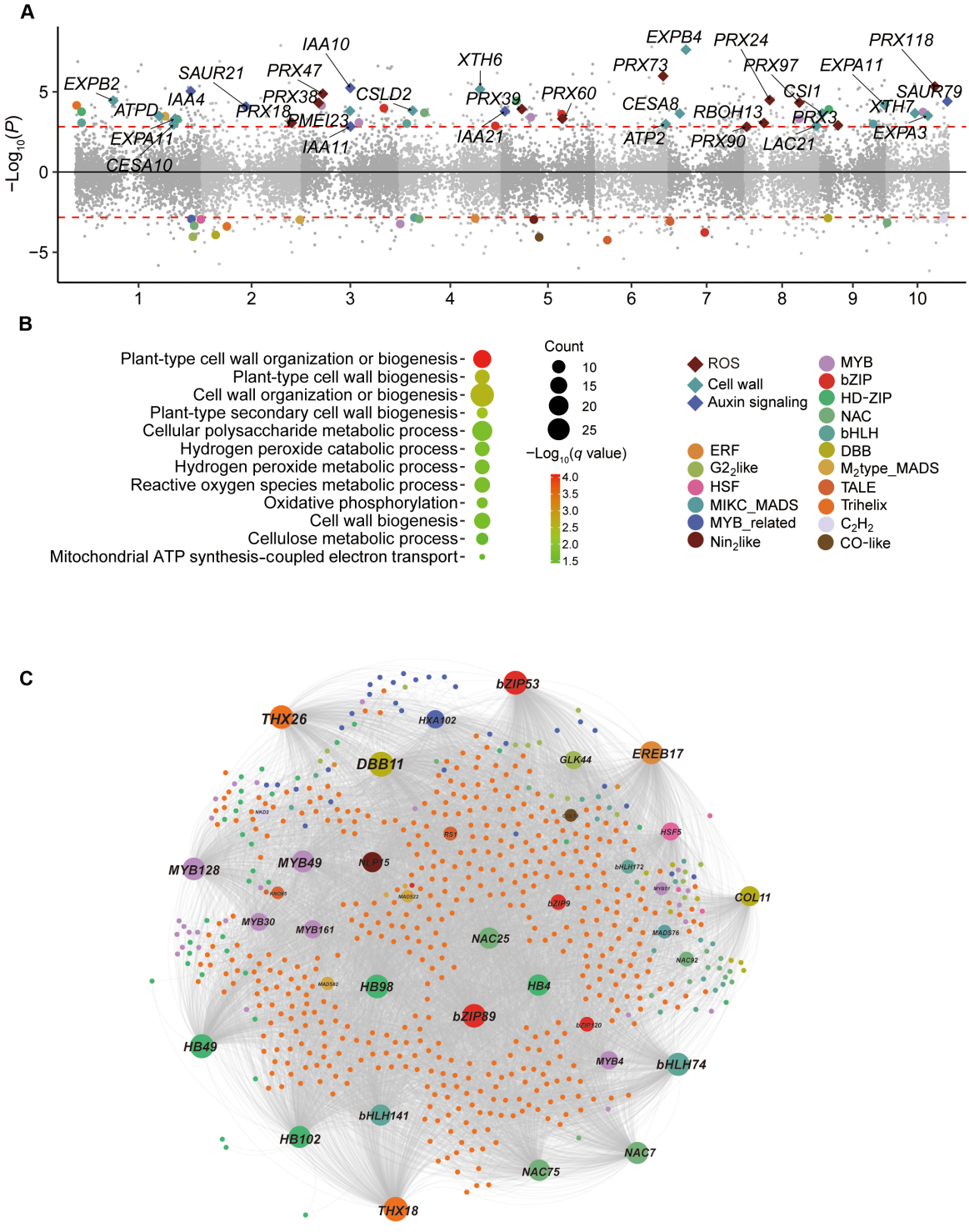

Fig. 1. TWAS for LRL. (**A**) Manhattan plot of TWAS results for LRL. Each point represents a single gene. Genomic positions of genes are plotted on the *x* axis, and $-\log_{10}$-transformed *P* values of the association between gene expression and LRL are plotted on the *y* axis. Genes positively and negatively associated with LRL are plotted above and below the red line, respectively. Colored dots represent different TF families. Brown, dark green, and blue diamond represent genes related to ROS, cell wall, and auxin signaling. (**B**) GO enrichment analysis of LRL-associated genes identified by TWAS. Dot size and color indicate the gene number and the range of FDR values, respectively. (**C**) Coexpression network of LRL-associated TFs and LRL-associated genes. Nodes are labeled with TFs names; the dot size reflects the number of target genes. Transcription factor and target genes are connected by undirected edges. Colored dots represent various TF families and their associated target genes. Orange dots represent target genes associated with multiple TFs.

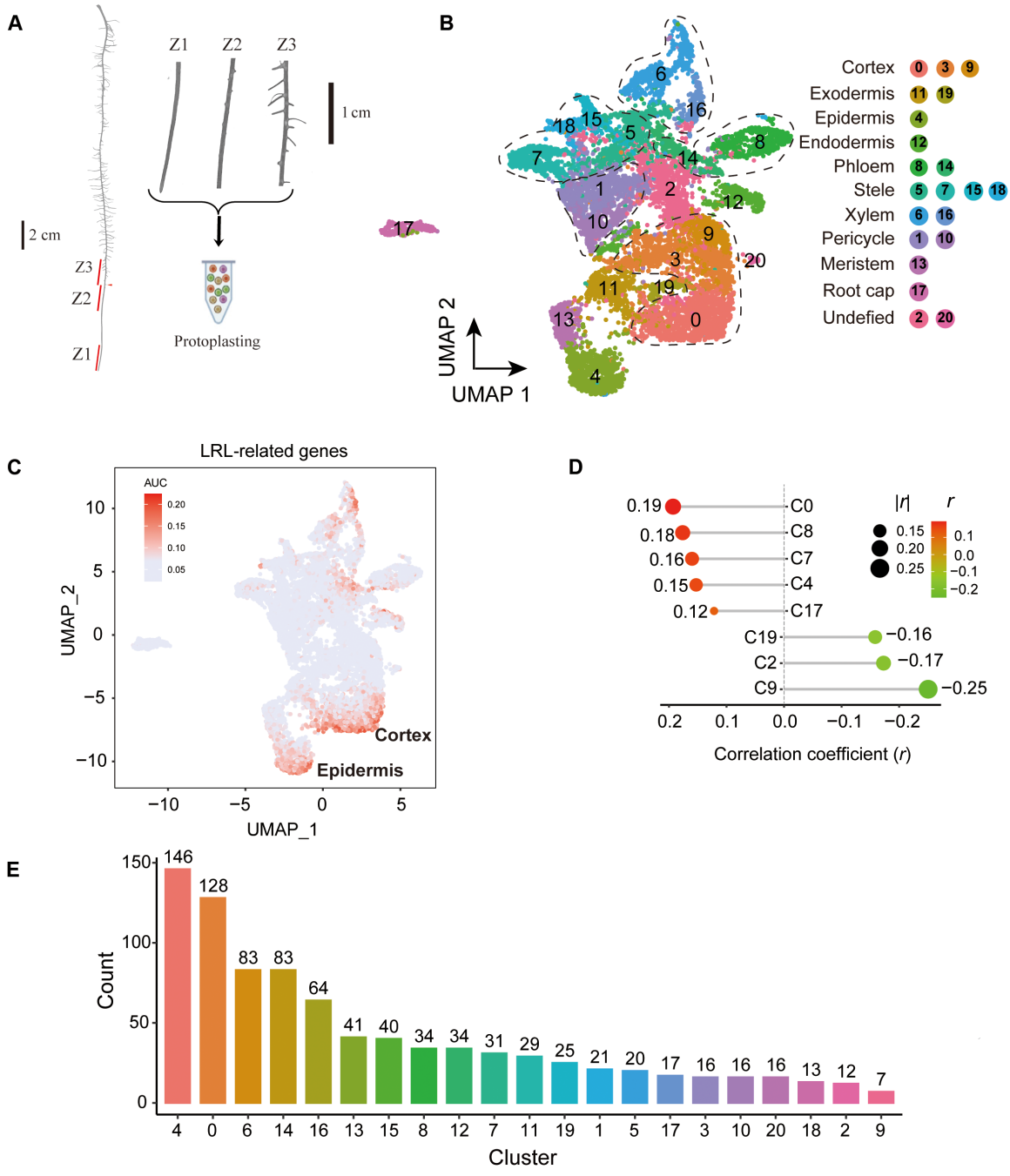

Fig. 2. LRL-associated genes enriched in the epidermis and cortex. (**A**) Overview of the scRNA-seq libraries generated using protoplasts isolated from the maize primary root. (**B**) UMAP visualization of putative clusters in the maize root. Each dot represents a single cell. Colors in the diagram of the root tip indicate the corresponding cell clusters. (**C**) UMAP plot with AUCell scores of LRL-associated genes in different cell clusters. (**D**) Pearson correlation between LRL and the cell fraction of each cluster. (**E**) Distribution of LRL-associated genes in different cell clusters. The bar plot indicates the number of genes in different cell clusters.

(GO: 0004601), and ROS metabolic processes (GO: 0072593) (tables S10 and S11). Considering root cell type–specific functions and developmental identities, we next aimed to link the single-cell gene expression atlas with specific cell-determined root traits (e.g., LRL). We first applied the deconvolution method to estimate the cell fractions of the bulk RNA-seq data for each inbred line, after which we analyzed the correlation between LRL and the cell fraction of each cluster. There were significantly positive correlations between LRL and C0 ($r = 0.19$, $P = 2.78 \times 10^{-4}$), C8 ($r = 0.18$, $P = 9.21 \times 10^{-4}$), C7 ($r = 0.16$, $P = 2.67 \times 10^{-3}$), C4 ($r = 0.15$, $P = 4.13 \times 10^{-3}$), and C17 ($r = 0.12$, $P = 2.27 \times 10^{-2}$) but negative relationships with C9, C2, and C19 (Fig. 2D). Together, these results suggest that cell type–specific genes, especially genes in epidermis and cortex, might play important roles in regulation of root length in maize.

ZmbZIP89 is a key regulator of LRL

Among the 37 TF genes associated with LRL, *ZmHB49*, *ZmbZIP89*, *ZmEREB17*, *ZmNAC25*, *ZmbHLH141*, *ZmMYB161*, *ZmbZIP120*, and *ZmCOL18* were predominantly expressed in clusters C0 or C4 (figs. S5 and S6). These TF genes may be coexpressed with 587 LRL-associated genes, with 449 (*ZmHB49*), 433 (*ZmbZIP89*), 407 (*ZmEREB17*), 344 (*ZmNAC25*), 338 (*ZmbHLH141*), 222 (*ZmMYB161*), 89 (*ZmbZIP120*), and 12 (*ZmCOL18*) target genes (table S5). To test whether these regulons [TFs with their direct-binding targets, expressed as TF (ng)] were specifically expressed in particular cell clusters, each regulon was set as the input for AUCell scoring. This analysis revealed that seven regulons [excluding COL18_extended (12 g)] were mainly expressed in C0 and C4 (fig. S7). Furthermore, we used the XGBoost algorithm to prioritize the most important TFs in C0 and C4. The feature importance scores, which reflect the significance of each TF in the prediction, were extracted from the XGBoost model. Among the eight analyzed TF genes, the potentially pleiotropic genes *ZmbZIP120*, *ZmbZIP89*, and *ZmCOL18* had the highest feature importance scores (Fig. 3A). Considering both the feature importance scores of TFs and the number of target genes, *ZmbZIP89* emerged as the key TF in C0 and C4 (Fig. 3, A and B).

To explore how *ZmbZIP89* contributes to lateral root development, we generated *ZmbZIP89* overexpressing (OE) lines using a *ZmUbi* constitutive promoter. Two independent lines, OE-1 and OE-2, in which the expression of *ZmbZIP89* was approximately 13-fold higher than that in the wild type (WT), were selected for further analyses (fig. S8A). The root lengths of the WT and OE lines were analyzed at the seedling stage. Compared to the WT, *ZmbZIP89*-OE plants exhibited a significant ($P = 1.17 \times 10^{-7}$) increase (~30%) in LRL, as well as total root length (TRL), primary root length (PRL), and seminal root length (SRL) (Fig. 3, C and D, and figs. S8B and S9). OE plants showed a notable enhancement in both average LRL in primary roots (APLRL) and lateral root density (PLRD) in primary root compared to the WT (Fig. 3F). Specifically, OE plants demonstrated approximately a 30% increase in LRL, a 21% increase in PLRD, and an impressive 110.8 to 187.2% increase in APLRL. These findings suggest that *ZmbZIP89* positively regulates lateral root development.

ZmbZIP89 directly regulates *ZmPRX47* expression

To clarify the molecular mechanisms underlying *ZmbZIP89* regulated lateral root development, a DNA-affinity purification sequencing (DAP-seq) analysis of ZmbZIP89 was performed to screen for its direct binding genes (table S12). Considering that genes directly targeted by a TF should be coexpressed in the same cell types, genes in the epidermis (C4) and cortex (C0) that were coexpressed with *ZmbZIP89* were extracted from the scRNA-seq data to narrow down the list of potential ZmbZIP89 targets involved in the regulation of root development. We then integrated the results of TWAS, DAP-seq, scRNA-seq, and gene coexpression analysis. Specifically, the LRL-associated genes identified by TWAS that were also detected as potential targets according to the gene coexpression analysis and DAP-seq analysis of *ZmbZIP89* were examined in terms of their expression in specific cell types using scRNA-seq data. A total of 86 target genes of *ZmbZIP89* were potentially involved in the regulation of lateral root development in the epidermis (C4) and cortex (C0) (Fig. 4A and table S13). A GO enrichment analysis indicated that these genes were significantly associated with multiple processes, including plant-type cell wall organization or biogenesis (GO: 0071554) and ROS metabolic process (GO: 0072593) (Fig. 4B and table S14). The cell wall–related genes included *ZmCESA8*, *ZmCSLD2*, *ZmEXPA11*, *ZmPGL19*, *ZmXTH6*, *ZmGPX11*, *ZmATP2*, and *ZmCSI1*. ROS-related genes included *ZmPRX38*, *ZmPRX39*, *ZmPRX47*, *ZmSOD10*, and *ZmRBOH13* (table S13).

We observed that both *ZmbZIP89* OE lines exhibit significantly higher root POD activity in comparison to WT plants (Fig. 3G). The target gene, the *ZmPRX47*, which encodes a POD, was significantly up-regulated in OE plants in comparison to WT (Fig. 4C). In addition, the expression level of *ZmbZIP89* was highly correlated with *ZmPRX47* ($P = 1.15 \times 10^{-8}$; Fig. 4A and table S6). To verify that *ZmPRX47* is directly targeted by ZmbZIP89, we analyzed the promoter region of *ZmPRX47*, which revealed a DAP-seq peak in a region [−476 to −212 base pair (bp)] upstream of the transcription start site (Fig. 4D). We next performed a dual-luciferase (LUC) reporter assay to determine whether ZmbZIP89 can bind to the *ZmPRX47* promoter and regulate its transcription in vivo. *LUC* expression driven by the 2-kb *ZmPRX47* promoter increased significantly when the reporter was cotransformed with the *ZmbZIP89* effector in *Nicotiana benthamiana* leaves (Fig. 4E). Furthermore, we constructed two pAbAi vectors containing the −476- to −322-bp and −322- to −212-bp *ZmPRX47* promoter regions corresponding to the DAP-seq peak. After ruling out self-activation, the −322- to −212-bp promoter region of *ZmPRX47* was used for a yeast one-hybrid (Y1H) assay, which detected a positive interaction with ZmbZIP89 (Fig. 4F). A well-known bZIP TF binding motif, CACGT, was detected in this promoter region. An electrophoretic mobility shift assay (EMSA) using a labeled probe with the CACGT motif from the *ZmPRX47* promoter (−322 to −302 bp) showed that recombinant ZmbZIP89-His can bind to the labeled probe, but not the mutated probe (Fig. 4G). Together, our findings suggest that ZmbZIP89 can directly activate *ZmPRX47* transcription.

ZmPRX47 regulates ROS production and lateral root development in maize

Integrative TWAS and single-cell analyses showed that *ZmPRX47* was specifically expressed in the cortex and epidermis, and its expression level was associated with LRL ($q = 0.0039$; Fig. 5A, fig. S10, and table S4). To assess whether *ZmPRX47* regulates LRL, we generated two independent mutants (*prx47#1* and *prx47#2*) using CRISPR-Cas9 technology. The *prx47#1* and *prx47#2* mutant plants contained 8-bp and two 1-bp mutations, respectively, resulting in premature termination (fig. S11). Knocking out of *ZmPRX47* resulted in an approximately 21% decrease in LRL, a 21.2 to 24.1% decrease in APLRL (Fig. 5, B to D), and a 17.1 to 23.3% decrease in PLRD (Fig. 5, B and E, and fig. S12). Moreover, POD activity was significantly lower in the *ZmPRX47* mutants than in WT plants (Fig. 5F). Notably, ROS signals in the lateral root primordia regions were stronger in the *ZmPRX47* mutants than in the WT plants (Fig. 5, G and H). Collectively, these results suggest a mechanism in that *ZmPRX47* might play a critical role in regulating ROS homeostasis, thereby inhibiting lateral root development.

ZmbZIP89-ZmPRX47 regulates drought tolerance in maize

The plant root system architecture has a crucial role in adaptation to drought stress. Both *ZmbZIP89* and *ZmPRX47* were mainly expressed in the root, with their expression being suppressed in response to drought stress (fig. S13). To determine whether *ZmbZIP89*

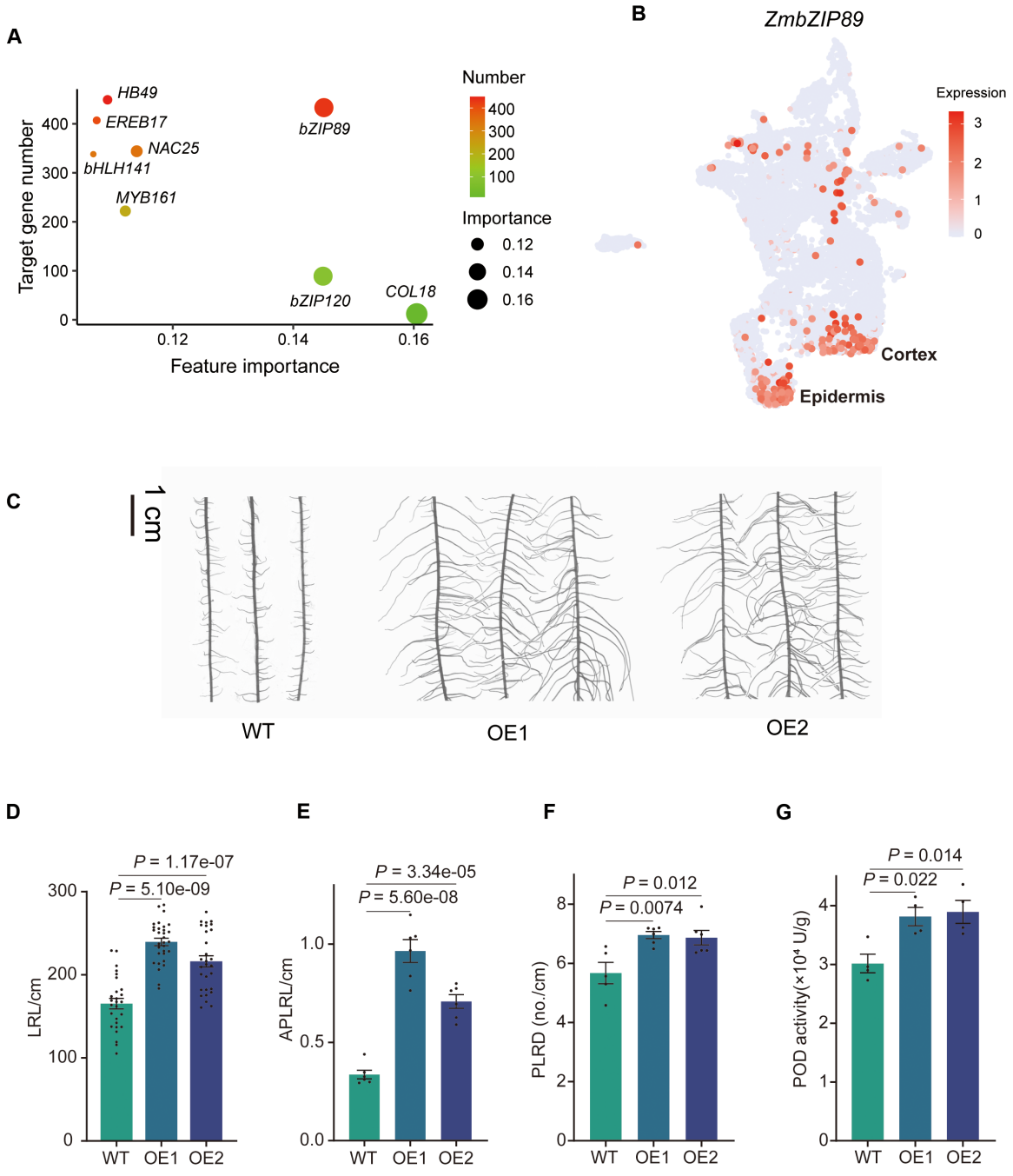

Fig. 3. *ZmbZIP89* positively regulates the LRL in the epidermis and cortex. (**A**) Transcription factors ranked by feature importance and number of target genes. Dots size represents the feature importance calculated by XGBoost, with colors ranging from green to red indicating the number of target genes. (**B**) UMAP plot showing *ZmbZIP89* expression in 21 cell clusters. (**C**) Root phenotypes of WT (ND101) and *ZmbZIP89*-OE lines at 14 days after germination in a hydroponic culture. (**D**) Statistical analyses of the LRL of WT ($n = 27$) and *ZmbZIP89*-OE plants ($n = 30$ and 28 for OE1 and OE2, respectively). (**E**) Average LRL on the primary root (APLRL) of WT and *ZmbZIP89*-OE plants ($n = 6$). (**F**) Lateral root density on the primary root (PLRD) of WT ($n = 5$) and *ZmbZIP89*-OE plants ($n = 6$). LRD was calculated according to the number of lateral roots per centimeter of primary root. (**G**) POD activity of WT and *ZmbZIP89*-OE plants ($n = 4$). Significance was evaluated by a one-way analysis of variance with Tukey's multiple comparisons test; *P* values are indicated.

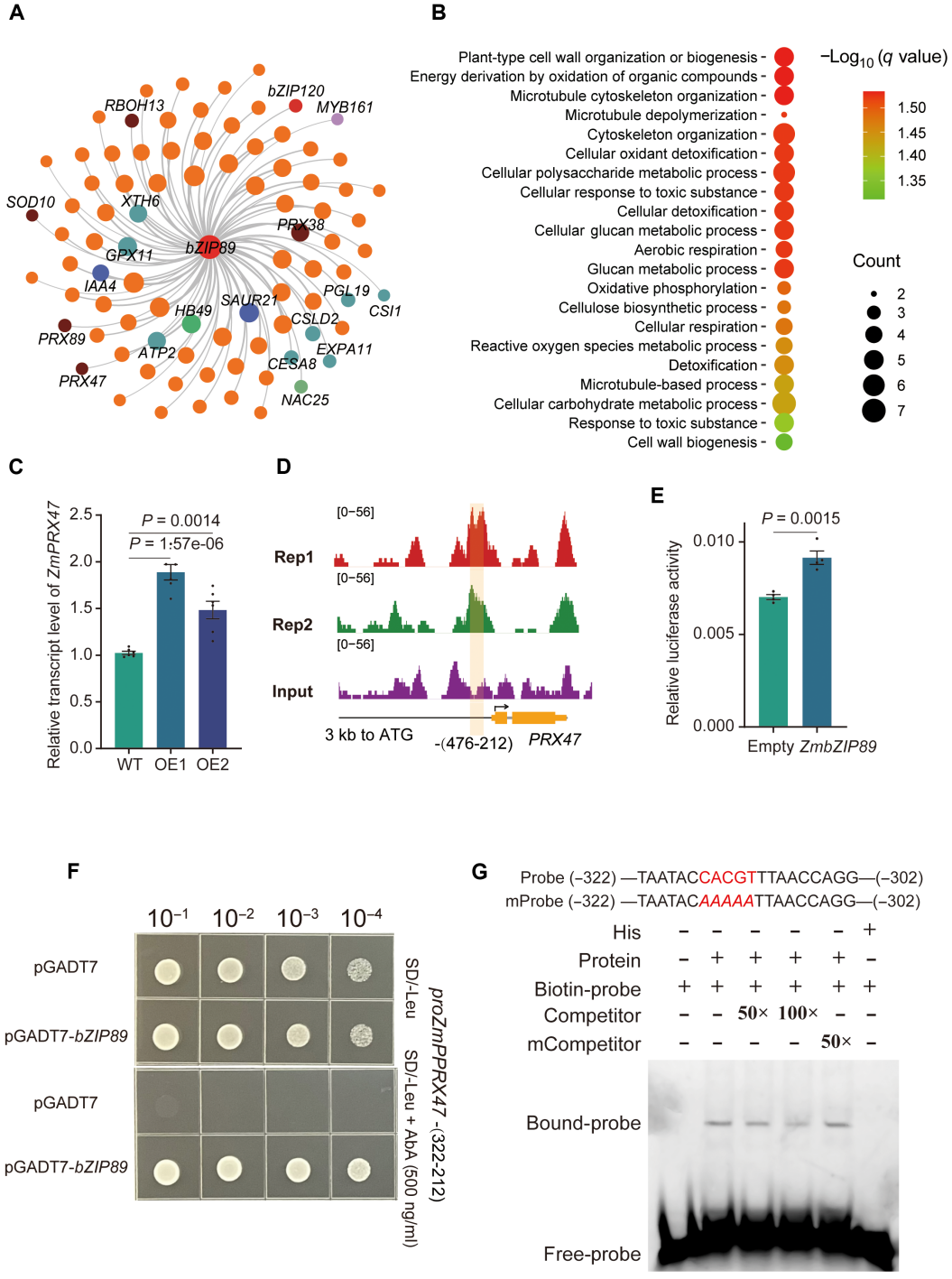

Fig. 4. Identification of the genome-wide direct targets of ZmbZIP89 in the epidermis and cortex. (**A**) Coexpression network of *ZmbZIP89* and 86 LRL-associated genes in cluster 0 or 4. Brown, dark green, and blue dots represent genes related to ROS, cell wall, and auxin signaling, respectively. Transcription factors are indicated by various colored dots, whereas other genes are indicated by orange dots. Dot size and the distance from the center represent the absolute value of the correlation coefficient (|*r*|) between target genes and *ZmbZIP89*. (**B**) GO enrichment analysis of *ZmbZIP89* target genes. Dot size and color indicate the number of genes and FDR values, respectively. (**C**) Relative *ZmPRX47* transcript level in WT and *ZmbZIP89*-OE plants ($n = 6$). Significance was evaluated by a one-way analysis of variance with Tukey's multiple comparisons test. (**D**) DAP-seq peak distribution of the ZmbZIP89-binding site in the *ZmPRX47* promoter. The orange shadow indicates the DAP-seq peak in the *ZmPRX47* promoter. (**E**) ZmbZIP89 activates the *ZmPRX47* promoter according to a transient dual-luciferase (LUC) assay ($n = 4$). Data are presented as the means ± SD from four independent replicates. Statistical significance was determined by a two-sided *t* test. (**F**) Y1H analysis of ZmbZIP89 directly targeting the *ZmPRX47* promoter fragment. Prey vector, *pGADT7-ZmbZIP89*; bait vector, pAbAi-$_{Pro}$*ZmPRX47*. Cotransformed yeast competent cells were grown on SD/−Leu medium with or without AbA (500 ng/ml). An empty pGADT7 vector served as the negative control. (**G**) EMSA results indicating that His-ZmbZIP89 can bind directly to the CACGT motif-containing regions of the *ZmPRX47* promoter. "+," presence; "–," absence; 50- and 100-fold excesses of unlabeled probes and mutant probes were used as competitors. His was used as the negative control.

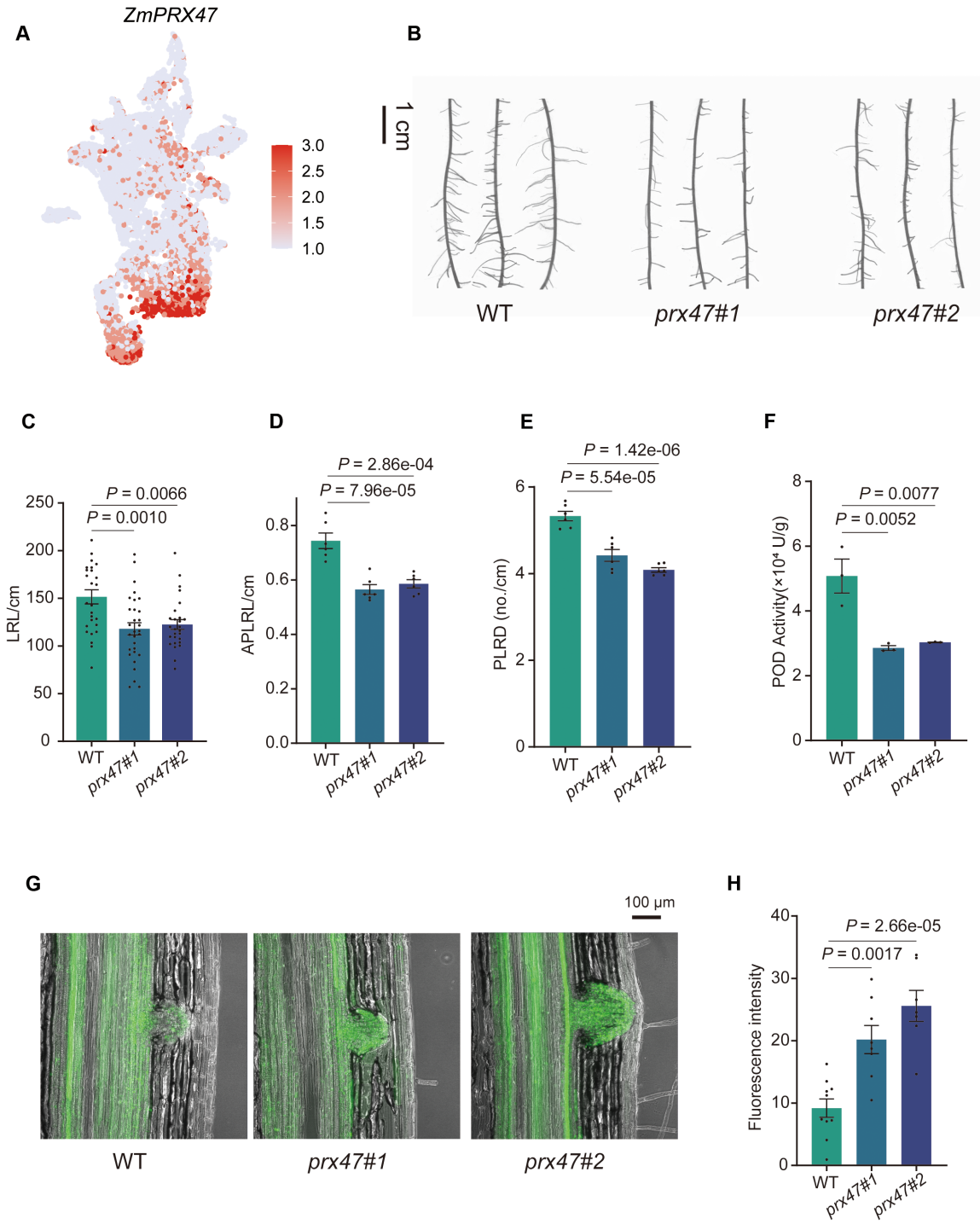

Fig. 5. *ZmPRX47* positively regulates the LRL in the epidermis and cortex. (**A**) UMAP plot showing *ZmPRX47* expression in the 21 cell clusters. (**B**) Root phenotypes of WT (KN5585) and *ZmPRX47* mutant plants at 14 days after germination in a hydroponic culture. (**C**) Statistical analyses of the LRL of WT and *ZmPRX47* mutant plants ($n = 24$). (**D**) Average LRL on the primary root (APLRL) of WT and *ZmPRX47* mutant plants ($n = 6$). (**E**) Lateral root density on the primary root (PLRD) of WT and *ZmPRX47* mutant plants ($n = 6$). LRD was calculated according to the number of lateral roots per centimeter of the primary root. (**F**) POD activity of WT and *ZmPRX47* mutant plants ($n = 3$). (**G**) Staining of ROS by H_2DCFDA. (**H**) Quantitative readout of the fluorescence intensity of H_2DCFDA in the lateral root primordium ($n = 10$, 8, and 7 for WT, *prx47#1*, and *prx47#2*, respectively). Significance was evaluated by a one-way analysis of variance with Tukey's multiple comparisons test; *P* values are indicated.

and *ZmPRX47* contribute to drought tolerance in maize, a soil cultivation box experiment with WT and transgenic lines was conducted under well-watered and drought conditions. Under drought conditions, *ZmbZIP89* OE lines consistently exhibited superior tolerance compared to WT plants (fig. S14). Following exposure to drought stress and a recovery period, the survival rate of WT was 46.2%, in contrast to 92.9 to 97.0% for overexpression lines (Fig. 6, A and C). In addition, the LRL and biomass of OE lines were significantly increased than WT plants (Fig. 6, B and D, and figs. S14 and S15). Furthermore, we compared the water use efficiency (WUE) of the transgenic and WT maize seedlings. The plant leaf photosynthetic rate (PS), stomatal conductance (SC), and transpiration rate (TR) were recorded at DAP15. Significantly higher PS, SC, TR, and WUE (calculated as PS in relation to TR) were observed in the transgenic plants under drought stress conditions (Fig. 6E and fig. S16). In addition, following the drought treatment, the *ZmbZIP89*-OE lines had significantly higher POD activities and less H_2O_2 than the WT (fig. S17). In a separate experiment for *ZmPRX47*, the survival rate of WT plants was 88.1%, whereas that of *prx47#1* and *prx47#2* was 11.1 and 8.2%, respectively (Fig. 6, F and H, and fig. S18). Compared with WT plants, the mutants had significantly low LRL, biomass, PS, SC, TR, and WUE under drought conditions (Fig. 6, G, I, and J, and figs. S18 to S20). The mutants also had significantly lower POD activities, which resulted in higher H_2O_2 levels than WT plants under drought conditions (fig. S21). Overall, these morphological and physiological analyses demonstrated that the ZmbZIP89-ZmPRX47 module systematically affects maize drought tolerance and recovery from drought stress.

Natural variation in the 3′UTR of *ZmbZIP89* confers lateral root development and drought tolerance

Last, we explored the natural variation of *ZmbZIP89* in association with LRL and drought tolerance among 164 resequenced maize inbred lines. According to an association analysis, 10 variants were significantly associated with *ZmbZIP89* expression, including one single-nucleotide polymorphism (SNP) in an intron, three synonymous SNPs, as well as four InDels and two SNPs in the 3′UTR (Fig. 7A). Because variants in the genic region did not alter the amino acid sequence, we focused on variant sites within the 3′UTR. Six variants in this region exhibited complete linkage disequilibrium, forming two distinct haplotype groups among maize inbred lines (Fig. 7B and fig. S22). The germplasms harboring the Hap2 allele had a substantially higher expression level ($P = 9.60 \times 10^{-6}$) and longer lateral root ($P = 1.70 \times 10^{-5}$) than those carrying the Hap1 allele, indicating that these variants may affect gene expression and LRL (Fig. 7C). To further examine the differences in drought resilience between Hap1 and Hap2 genotypes, we analyzed a representative number of randomly selected lines carrying each haplotype. SDW, PS and WUE were higher in the inbred lines with Hap2 than in the inbred lines carrying Hap1 (Fig. 7, D to G, and fig. S23).

To determine whether this variant affected *ZmbZIP89* mRNA abundance, we cloned the 3′UTR sequence of inbred lines with Hap1 and Hap2 (fig. S24). Transient transcriptional activation experiments showed that the Hap2 exhibited significantly stronger transcriptional activity than that with Hap1 (Fig. 7H), indicating that the natural variation in the 3′UTR influenced *ZmbZIP89* expression. Further, we explored the *ZmbZIP89* mRNA stability of the two haplotype groups in *N. benthamiana* leaves. $ZmbZIP89^{hap2}$ mRNA degraded more slowly than $ZmbZIP89^{hap1}$ mRNA, which was consistent with the observed differences in *ZmbZIP89* mRNA stability in the roots of maize inbred lines containing Hap1 and Hap2. Accordingly, the 3′UTR of $ZmbZIP89^{hap2}$ might be more favorable for the mRNA stability than that of $ZmbZIP89^{hap1}$ (Fig. 7I and fig. S25). We further analyzed the sequence variance of gene *ZmbZIP89* among 189 teosinte accessions and 507 inbred lines (*24*). The drought-resistant allele at SNP1419 was less frequent (42%) than the drought-recessive allele (58%) among the sequenced teosinte accessions (Fig. 7J). A similar pattern was observed for SNP1400 in the 3′UTR, with the resistant allele at 48.3% (fig. S26). In contrast, maize inbred lines showed a marked increase in the frequency of drought-resistant alleles, reaching 86.1% for SNP1419 and 89.1% for SNP1400, indicating strong selection for these alleles during modern breeding.

DISCUSSION

Lateral root establishment and patterning are crucial for shaping the overall root system architecture, enabling adaptations to soil stress (*3*, *25*), and ultimately influencing cereal crop performance and productivity (*26*–*28*). Lateral root emergence is determined by sequential spatiotemporal cellular events involving the pericycle, endodermis, cortex, and epidermis in maize (*13*). Such a developmental process is regulated by genetic factors and modulated by environmental constraints (*3*, *22*, *29*). However, little is known about how the cellular determination and the associated molecular mechanisms affect root system establishment and function. In addition, it remains unclear how extensively lateral root traits influence stress resilience, especially in crops. Addressing these knowledge gaps is essential for fully characterizing root developmental plasticity and the capacity to adapt to climate changes with adverse effects on agriculture.

We conducted a population-based TWAS and scRNA-seq analysis of maize. Our results suggest that cortex and epidermis cell types play important roles in lateral root elongation, thus contributing to the overall absorption surface of the root system (Fig. 2). To date, only two maize genes, *RUM1* and *LRT1,* have been implicated in lateral root initiation. However, both genes exhibit severe pleiotropic effects, influencing not only root system but also leaf development (*29*, *30*). The pleiotropy may hinder the application of these genes for targeted engineering of specific root traits without negatively altering other traits, including yield. Notably, we here provide a single-cell transcriptional snapshot of gene expression in maize primary root, offering initial insights into maize lateral root development. This resource advances our understanding of the complex relationship between root architecture and cell identity in maize genetic populations. Moreover, it provides a foundation for future research on maize root development and function (Figs. 1 and 2).

Our integrative analysis combined with transgenic approaches identified a key root-specific TF *ZmbZIP89* as a key regulator of lateral root development and revealed its associated gene network involved in abiotic stress resistance (Figs. 3 and 6). Biochemical and molecular binding assays demonstrated that ZmbZIP89 can activate *ZmPRX47* expression, thereby regulating ROS homeostasis around the lateral root primordia while also likely facilitating lateral root primordial emergence through the cortex and epidermis (Fig. 5). Future studies, such as cell type–specific gene knockout experiments, should further elucidate the spatial and functional relationships among *ZmbZIP89*, *ZmPRX47*, and ROS production. The ZmbZIP89-ZmPRX47 module exhibits a highly root-specific expression pattern that promotes lateral root development and

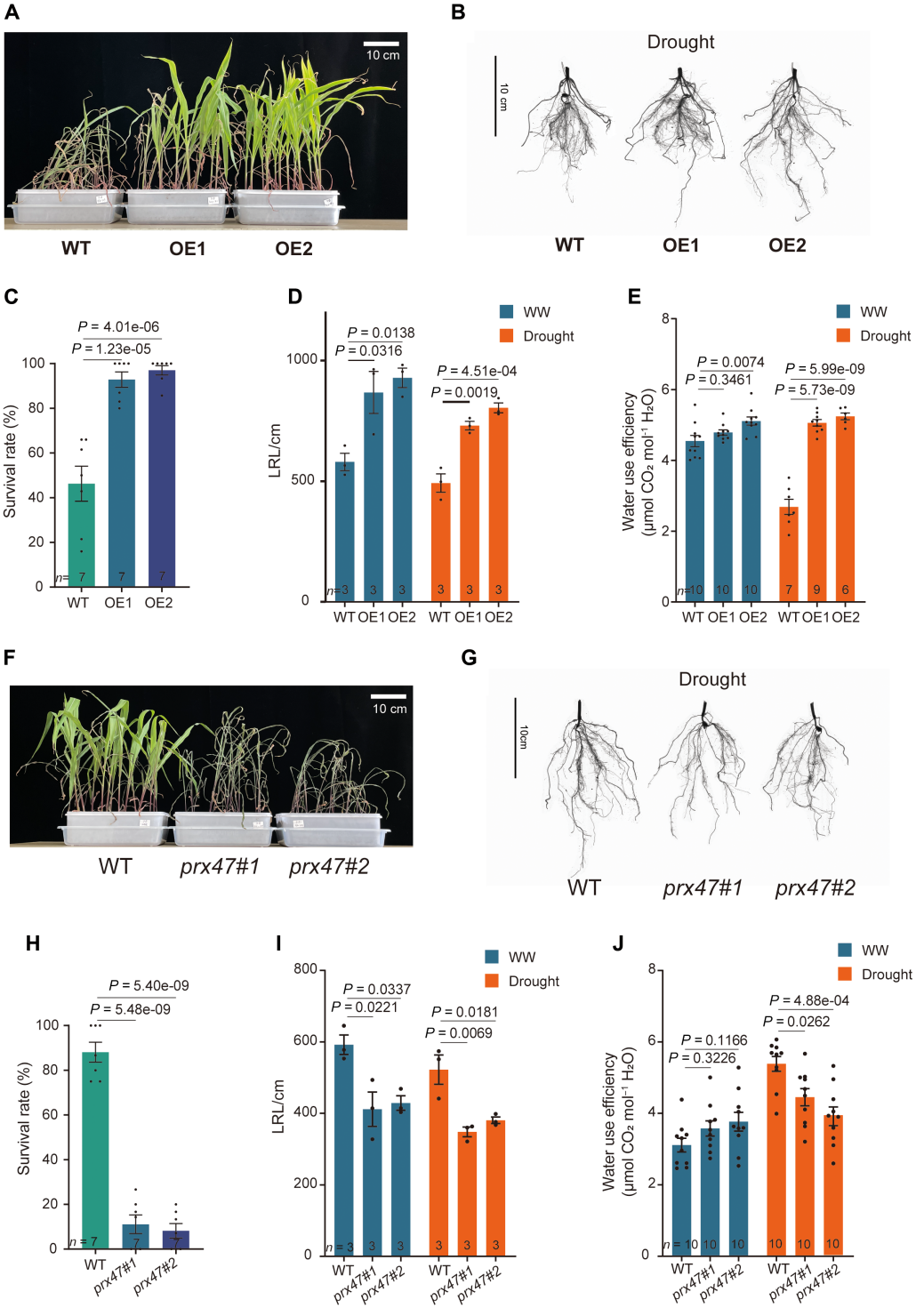

Fig. 6. Drought tolerance of *ZmbZIP89* and *ZmPRX47* transgenic maize. (**A**) Drought tolerance of *ZmbZIP89*-OE plants and the WT (ND101) control. Plants were photographed after a 23-day drought treatment followed by a 2-day of rewatering. (**B**) Root phenotypes of *ZmbZIP89*-OE plants and the WT control under drought conditions at 15 days after planting. (**C**) Statistical analysis of survival rates after the drought treatment and recovery period. (**D** and **E**) Statistical analysis of the LRL and WUE of *ZmbZIP89*-OE plants and WT plants under well-watered (WW) and drought conditions at 15 days after planting. (**F**) Drought tolerance of *ZmPRX47* CRISPR-knockout lines and the WT (KN5585) control. Plants were photographed after a 23-days drought treatment followed by 2-days of rewatering. (**G**) Root phenotypes of *ZmPRX47* CRISPR-knockout lines and the WT control under drought conditions at 15 days after planting. (**I**) Statistical analysis of survival rates after the drought treatment and recovery period. (**H** and **J**) Statistical analysis of LRL and WUE of *ZmPRX47* CRISPR-knockout lines and the WT plants under well-watered and drought conditions at 15 days after planting. Genotypic differences within each treatment group were evaluated by a one-way analysis of variance with Tukey's multiple comparisons test.

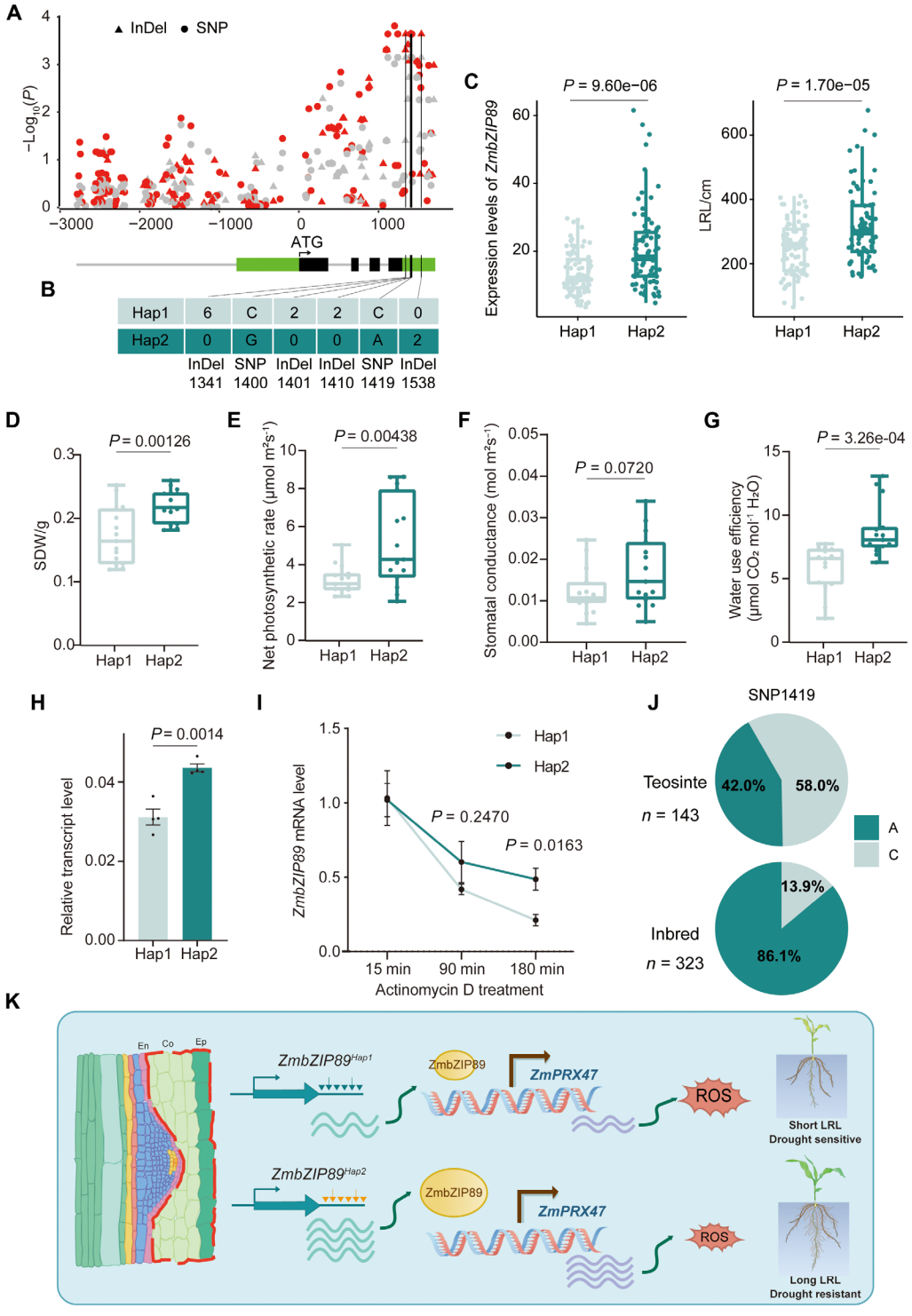

Fig. 7. Natural variation in the 3′UTR of *ZmbZIP89* confers robust lateral root development and enhanced drought tolerance. (**A**) Analysis of the association between the genetic variation in *ZmbZIP89* and the *ZmbZIP89* expression level (red) and LRL (gray); circles and triangles represent SNPs and InDels, respectively. (**B**) Haplotypes of variations in the *ZmbZIP89* 3′UTR. (**C**) Relative *ZmbZIP89* expression levels (left) and LRLs (right) for Hap1 ($n = 86$) and Hap2 ($n = 78$). (**D** to **G**) Statistical analysis of the shoot dry weight (SDW), PS, SC, and WUE for Hap1 ($n = 15$) and Hap2 ($n = 15$) under drought conditions at 15 days after planting. (**H**) Transcript levels of *LUC* (firefly luciferase) in *N. benthamiana* leaves transformed with Hap1 3′UTR and Hap2 3′UTR ($n = 4$). (**I**) mRNA degradation assay involving different 3′UTR sequences. *ZmbZIP89* mRNA abundance after a treatment with a transcription inhibitor (actinomycin D), relative to the abundance before the treatment. Data are represented as the means ± SD from four biological replicates. Statistical significance was determined by a two-sided *t* test. (**J**) Distribution frequency of SNP1419 in teosinte and inbred lines. (**K**) Model depicting a *ZmbZIP89-ZmPRX47* module regulating lateral root development and drought resilience in maize. Natural variations in the 3′UTR of *ZmbZIP89* enhance gene expression by increasing mRNA stability, leading to increases in the LRL and drought tolerance.

contributes to ROS homeostasis, which is associated with enhanced abiotic stress resistance (*31*, *32*). A strong root system is conducive to the absorption of water from the soil and improves drought resistance (*33*); however, under well-watered conditions, a significant portion of the root system may be functionally redundant in terms of water uptake. In drying soil, root morphological and anatomical traits as well as the expression levels of active aquaporin genes become increasingly important for maintaining WUE when the water supply is limited (*34*). Therefore, an increase in LRL in the *ZmbZIP89*-OE lines could help improve water acquisition, especially under drought conditions. A lack of a significant improvement in WUE under well-watered conditions (Fig. 6E) may be because water uptake is not a limiting factor, thus masking the potential benefits of increased LRL on WUE. A similar result was observed for *ZmVPP1*, which reportedly enhances drought tolerance by promoting root development. When the soil water content is approximately ~15 to ~25%, WUE increases in *ZmVPP1*-OE lines in comparison to the WT (*28*). In plants, ROS scavenger are important for drought tolerance by protecting plant cells from oxidative damage and maintaining cellular homeostasis (*31*, *32*). However, ROS production and lateral roots formations might hinder the causal relationship between root architecture and drought resistance, which may be related to the complexity of the relationship between lateral root development and ROS signaling in plants (*35*). Future research will need to elucidate the effects of single gene-mediated root developmental plasticity and hydraulic architecture on soil water uptake and plant use efficiency.

According to recent findings, the maize root system was domesticated during the global adaptation to soil water availability (*8*). Specifically, the natural variation in *ZmHb77* (encoding homeobox-TF 77) is associated with root architecture and drought tolerance. In addition, *ZmHb77*-driven domestication and establishment of the root system significantly affect the root system architecture and lateral root patterning (*8*). We determined that an independent mechanism involving *ZmbZIP89* regulates lateral root elongation and potential root ROS dynamics. Both *ZmHb77* and *ZmbZIP89* represent convergent regulatory pathways for root traits that significantly influence maize drought tolerance and resilience in natural populations (Fig. 7K) (*8*). Nevertheless, future studies should clarify the spatial patterns of gene-gene interactions influencing root physiology and developmental states. Doing so may facilitate a systematic characterization of specific root traits mediating abiotic stress resistance in cereal crops. The developmental states of all major cell types must be precisely resolved for a comprehensive understanding of root system development and adaptation to abiotic stress. Last, in the current study, we revealed an important TF that determines root development in maize, with potential implications increasing crop drought resilience via genetic engineering for sustainable agriculture.

MATERIALS AND METHODS

Plant cultivation and traits measurements

The 357 maize accessions used in this study (table S1), comprised 213 inbred lines from an association-mapping population (*36*), 23 founders of the CUBIC population, and 121 progenies randomly sampled from the CUBIC population (*37*). All genotypes were cultivated using a paper-roll–based hydroponic system (*36*). Briefly, seeds with a uniform size were surface sterilized during a 20-min treatment with 10% H_2O_2. Seeds were rinsed twice with distilled water and then immersed in a saturated $CaSO_4$ solution for 6 hours. They were then germinated in darkness on moistened filter paper at 28°C and 80% relative humidity. After 48 hours, eight germinated seeds per genotype were vertically rolled within two layers of brown germination paper (Anchor Paper Company, St. Paul, MN, USA). The paper rolls were placed in black incubators (39.5 cm by 29.5 cm by 22.5 cm) containing 7.5 liter of nutrient solution. The nutrient solution consisted of 2.0 mM $Ca(NO_3)_2$, 0.75 mM K_2SO_4, 0.65 mM $MgSO_4$, 0.1 mM KCl, 0.25 mM KH_2PO_4, 1×10^{-3} mM H_3BO_3, 1×10^{-3} mM $MnSO_4$, 1×10^{-4} mM $CuSO_4$, 1×10^{-3} mM $ZnSO_4$, 5×10^{-6} mM $(NH_4)_6Mo_7O_{24}$, and 0.1 mM Fe-EDTA (*36*). The nutrient solution was renewed every 3 days and continuously aerated using an electric pump. Plants were grown in a greenhouse at Yangzhou University in May 2019. The experiment was conducted using a completely randomized design with two replicates. Seedlings were harvested at 14 days after germination, and the roots were separated from the shoots. For each genotype, six plants per replicate were harvested and stored at 4°C before scanning with high-resolution scanner (EPSON V800, Japan). High-quality images were analyzed using WinRHIZO software (Pro 2004b, Canada) to determine TRL. After measuring PRL and SRL using a ruler, LRL was calculated by subtracting PRL and SRL from TRL.

RNA-seq analysis, data processing, and gene expression quantification

For all 357 inbred lines, root tissue collected from three individual plants was pooled, immediately frozen in liquid nitrogen, and stored at −80°C. Total RNA was extracted from the frozen root samples using TRIzol reagent (Invitrogen). RNA sequencing libraries were prepared from the extracted total RNA using the TruSeq Paired-end mRNA-Seq Kit according to the manufacturer instructions (Illumina). Libraries were sequenced using the Illumina HiSeq 2500 system with Illumina TruSeq SBS v3 reagents. Raw reads were preprocessed using Trim-galore (v0.6.10) with parameters "-q 20 --stringency 3 --length 36" to remove the adapters and low-quality reads. High-quality reads were mapped to the Zm-B73-REFERENCE-NAM-5.0 (http://ftp.ensemblgenomes.org/pub/plants/release-52/fasta/zea_mays/dna/) reference genome using the default parameters (for RNA-seq) of HISAT2 (v2.1.1). Mapped counts per gene were calculated using featureCounts (v2.0.1) and normalized to TPM.

Transcriptome-wide association study for LRL

To conduct the TWAS analysis, genes with a TPM value greater than 0.5 in at least 80% of the accessions were retained (*38*, *39*). Association analyses were performed using EMMAX software with LMM (*40*). The following linear mixed model was used: $y \sim (\beta x, \sigma_G^2 K_G + \sigma_e^2 I)$.

Here, y denotes LRL across varieties, x denotes the expression levels of a gene across varieties, β is the effect of the gene on the phenotype, and K_G is the kinship matrix. The kinship coefficients were estimated using the centered-IBS (identity by state) method in TASSEL 5.2.92. FDR ≤ 0.05 was used as the significance threshold for TWAS (*38*).

Gene coexpression network analysis of bulk RNA-seq

To construct a TF-target gene regulatory network, Pearson correlation coefficients were calculated for the relationships between the expression levels of TF genes and target genes. Correlation coefficients and P values for each TF-target pair were calculated by the corr.test() function in the R package "psych." A stringent significance threshold of $P \leq 4.17 \times 10^{-7}$ was applied to define edges in the

network based on Bonferroni correction (α/n, where $\alpha = 0.01$ and n is the number of all edges: 37 TF genes × 647 target genes). The resulting gene coexpression network was visualized by Cytoscape (v3.5.0) software.

Gene functional analysis

A GO enrichment analysis was conducted using OmicShare tools (www.omicshare.com/tools). Significantly enriched GO categories were identified using a FDR ≤ 0.05 as the threshold.

scRNA-seq library preparation, sequencing, and data preprocessing

The inbred line B73 was used for the root scRNA-seq analysis. Seeds were germinated and grown under the same conditions as described for TWAS. At 10 days after germination, primary roots were harvested from 100 seedlings and dissected into three zones, which were based mainly on the emergence of lateral roots. More specifically, zone 1 was a 1-cm region from the root tip, whereas zones 2 and 3 were 1-cm regions below and above the point of the first lateral root, respectively (Fig. 2A). Root segments were cut into small pieces (1 to 2 mm) and incubated in 50 ml of enzyme solution containing 1.5% (w/v) cellulase R10, 0.7% (w/v) macerozyme R10, 0.1% (w/v) bovine serum albumin, 3 M KCl, and 0.5 mM MES-KOH (pH 5.7). The mixture was agitated at 60 rpm for 4 hours at 22°C in darkness to digest cell walls (*41*). Following digestion, cells were filtered through a 40-μm cell strainer (Falcon, 352340). Cell viability was assessed using trypan blue staining, and cell concentration was determined using a hemocytometer under a light microscope (Bio-Rad TC20). Protoplasts were resuspended in an 8% (w/v) mannitol solution before loading onto the chromium controller of the 10× Genomics platform. Approximately, 20,000 isolated single cells and enzyme gel beads were packed into a single oil droplet to construct the scRNA-seq library. Cells were loaded onto the 10× Chromium Single Cell Platform (10× Genomics) at a concentration of 700 to 1200 cells/μl (Single Cell 3′ library and Gel Bead Kit v.3) as described in the manufacturer's protocol. The final library was sequenced on the Illumina NovaSeq6000 platform by Shanghai Personalbio (Shanghai, China) using 150-bp paired-end reads.

Raw scRNA-seq reads data were aligned to the B73 reference genome (Zm-B73-REFERENCE-NAM-5.0) and counted using the Cell Ranger pipeline (v 6.0, 10× Genomics). The raw count matrix data were imported into R using the Seurat (v4.0) package for further data analysis (*42*). Cells with fewer than 200 detected genes and genes detected in fewer than three cells were removed (*17*). We also filtered the cells with unique gene counts more than 5000 or fewer than 500 to eliminate dead cells and doublets (*42*). Cells with more than 10% mitochondrial sequence were also removed (*43*). Last, we obtained 12,190 single cells for the downstream analyses. The dataset was scaled and normalized by the ScaleData and NormalizeData functions (*42*). The top 2000 highly variable genes were used for a principal components analysis (PCA). The first 20 principal components were selected according to the PCA elbow plot and used for clustering with a resolution parameter of 0.3 (*20*). Clusters were visualized and explored by UMAP (*44*). Cluster-specific marker genes were identified using the function FindAllMarkers in the Seurat package with min.pct = 0.25 and logfc.threshold = 0.25. Cluster annotations were compared according to the markers for cell type–specific genes in previous datasets (*17*, *45*, *46*).

Pseudo-time analysis and RNA velocity analysis

Cortex (clusters 0, 3, and 9) and stele (clusters 5, 7, 15, and 18) cells were selected for the reconstruction of the developmental trajectory by the Monocle2 package (v2.18.0). Highly variable genes were identified using the dispersiontable function. In addition, a dimensional reduction clustering analysis was performed with the reduceDimension function (max_components = 2, method = DDRTree), after which the trajectory was inferred using the orderCells function (default parameters). The trajectory was plotted by plot_cell_trajectory in Monocle 2 (*47*).

A single-cell trajectory analysis of cortex and stele cells was performed by RNA velocity using the scVelo python module (*48*). The spliced reads and unspliced reads were recounted on the basis of aligned bam files of Cell Ranger output. RNA velocities were calculated using the scvelo.tl.velocity function with default parameters and projected onto the UMAP embedding obtained in Seurat.

Bulk tissue cell-type estimation using CIBERSORTx deconvolution

To estimate the cellular composition of bulk RNA-seq data from 357 inbred lines, we used CIBERSORTx deconvolution (*49*). The top 50 genes that were highly expressed in each cell type were selected to construct the signature matrix. This signature matrix, along with the bulk RNA-seq expression matrix of the 357 inbred lines, served as the input for CIBERSORTx. Deconvolution was performed with 1000 permutations, while all other parameters were left at their default settings. The resulting cell fraction estimates were then correlated with LRL using Pearson correlation. A significance threshold of $P < 0.05$ was applied to identify cell types with a statistically significant correlation between their estimated fractions and LRL.

Gene set score by AUCell

AUCell is a method for identifying cells with an active gene set in single-cell RNA-seq data (*23*). The input for AUCell is a gene sets, whereas the output is the gene set "activity" [area under the curve (AUC)] in each cell. In this study, 647 LRL-associated genes were set as the input for calculating the AUC value. According to the AUC value, gene-expression rankings were built for each cell by the "AUCell_run" function in the AUCell package. The AUC estimates the proportion of genes in the gene set that are highly expressed in each cell. Cells expressing many genes from the gene set will have higher AUC values than those expressing fewer genes. The function "AUCell_exploreThresholds" was used to calculate the threshold for considering the current gene set active. Then, cell clustering UMAP embedding was colored on the basis of the AUC score of each cell to show which cell clusters were active in the LRL-associated gene set. For identifying cells with active gene regulatory networks for eight TFs, the input gene sets were the regulons.

DAP sequencing

DAP-seq analysis was conducted as previously described (*50*). Briefly, genomic DNA was extracted from the young roots of B73 seedlings, fragmented, and ligated with a truncated Illumina TruSeq adapter to construct a DAP-seq library. The full-length *ZmbZIP89* coding sequence (CDS) was subcloned into the pFN19K HaloTag T7 SP6 Flexi expression vector for the expression of ZmbZIP89 with an N-terminal HaloTag affinity tag in an in vitro Wheat Germ Extract System (Promega). Recombinant ZmbZIP89-HaloTag proteins

were directly captured using Halo Tag Beads (Promega). The beads bound with ZmbZIP89 were subsequently incubated with adapter-ligated guide DNA libraries in an incubation buffer composed of 1× PBS and 0.005% (v/v) IGEPAL CA-630. The mixture was slowly rotated for 2 hours at 4°C. The beads were washed three times with PBS, and then DNA fragments were eluted from the ZmbZIP89-HaloTag beads using an elution buffer consisting of 50 mM tris-HCl (pH 8.5). The eluted DNA was sequenced using the Illumina NovaSeq 6000 platform. The negative input control consisted of Magne Halo Tag Beads incubated with an adapter-ligated genomic DNA library. The analysis was completed using two technical replicates.

Raw reads were processed using Trim Galore (v0.6.10). Clean reads were mapped to the Zm-B73-REFERENCE-NAM-5.0 using Bowtie2 (v2.4.5). Mapped reads were then filtered using SAMtools (v1.6) to eliminate the reads aligned to multiple locations with the parameters: -h -q 30 -F 4 -F 256. Peaks calling was performed using MACS2 (v2.2.7.1) with the input DNA library serving as the control. The bam files were converted to bigwig files and visualized using Integrative Genome Browser (v2.15.4).

Machine learning models for trait prediction

A model for predicting phenotypes based on gene expression was constructed using an ensemble of gradient-boosted trees (XGBoost) (*51*). The 357 genotypes were initially partitioned into training and testing datasets, composing of 80 and 20% of the data, respectively. Testing samples were never used for training. Phenotypes were predicted using the Python machine learning libraries scikit-learn (v.1.4.1.post1) and XGBoost (v.2.0.3). The grid search algorithm was used to optimize hyperparameters in each iteration, which included colsample_bytree, learning_rate, max_depth, min_child_weight, n_estimators, and subsample. This process was repeated 100 times with different seeds to account for variations in the hyperparameter optimization procedure. To assess the stability of individual phenotype predictions, we computed the mean-squared error and R^2 values for the test set. Last, the importance of each gene was evaluated.

Generation of *ZmbZIP89*-OE and *ZmPRX47*–CRISPR-Cas9 transgenic maize lines

To generate *ZmbZIP89*-OE lines, the full-length *ZmbZIP89* CDS was cloned into the *pBCXUN* vector (*52*) to generate the *Ubi*:*ZmbZIP89* fusion construct. The recombinant was subsequently introduced into *Agrobacterium tumefaciens* strain EAH105 cells for the *A. tumefaciens*–mediated transformation of immature embryos of maize inbred line ND101 (*53*). The seeds of *ZmbZIP89*-OE lines were produced by the Crop Functional Genomics and Molecular Breeding Research Center at China Agricultural University. T_0 generation transgenic plants were selected after which T_3 seeds were produced through successive rounds of self-pollination. Homozygous T_3 seeds were used for phenotypic analyses. Gene expression levels in *ZmbZIP89*-OE lines were quantified via reverse transcription quantitative polymerase chain reaction (RT-PCR), with *ZmUbi2* serving as the internal control.

To generate *ZmPRX47* knockout lines using CRISPR-Cas9 technology, two target sites (CCTCTGCGCGCTTGTGGCTGTTC and CCGGTGAACATCGGGCTCGCAGC) in the first and second exons of *ZmPRX47* were obtained from CRISPR-P (http://crispr.hzau.edu.cn/CRISPR2/). Specific gRNAs were cloned into the ZmUbi-Cas9 vector via a recombination reaction using CloneExpress MultiS (Vazyme Biotech, Nanjing, China). Following the *A. tumefaciens*–mediated transformation of immature embryos from maize inbred line KN5585 by the Wimibio Company (Changzhou, China). Independent T_0 transgenic plants were identified by PCR genotyping of the *Bar* gene, and the gene-specific editing was detected according to a gene-specific PCR amplification and sequencing. The PCR primers used are listed in table S15. At least two independent knockout and Cas9-free T_1 lines were self-pollinated to obtain T_2 progeny, which were used for phenotypic analyses.

Evaluation of maize seedling root and drought tolerance

Root phenotypes of transgenic and WT plants were evaluated as described for TWAS. The lateral root primordium density of the primary root was evaluated at 4 days after germination. To evaluate drought tolerance, seeds of transgenic and WT plants were sown in cultivation boxes (length × width × depth: 30 cm by 20 cm by 10 cm) filled with 3.5 kg of mixed substrate (turf:vermiculite ratio of 8:1). After a 2-day germination period, 15 seedlings per line were transplanted into cultivation boxes for each replicate. Drought treatment was applied to the soil-grown plants at the three-leaf seedling stage by withholding water, with a soil water capacity of 20%. Approximately 15 days after planting, roots were washed and LRL, POD activity, and H_2O_2 content were measured. A LI-COR 6800 portable photosynthesis system was used to analyze PS and SC of the newest fully expanded leaves. After approximately 23 days, plants were rewatered, and then the survival rate was recorded 2 days later. Shoots were harvested to measure shoot fresh weight and dry weight. POD activity and H_2O_2 contents were measured using analytical kits supplied by Beijing Solarbio Science & Technology Co., Ltd.

ROS detection in lateral root primordia

Lateral root primordia were prepared by sectioning fresh maize roots into 50-μm segments using a Leica VT1200 S automatic vibrating slicer. The prepared sections were immediately immersed in 1× phosphate-buffered saline (PBS) solution for short-term storage. To visualize ROS levels in lateral root primordia, we used the ROS-sensitive probe H_2DCFDA. Specifically, root sections containing lateral root primordia were incubated with 5 μM H_2DCFDA in darkness at 37°C for 1 hour. They were washed at least three times and then examined for H2DCFDA-related enhanced green fluorescent protein fluorescence using a confocal laser scanning microscope (LSM710). Consistent exposure times were maintained across all experiments. ImageJ software was used to quantify the average fluorescence intensity within regions of interest.

Transient transcriptional activity assay

To determine whether ZmbZIP89 can activate *ZmPRX47* transcription, the *ZmPRX47* promoter region was amplified from maize B73 genomic DNA and then inserted into the pGreenII0800-LUC vector to produce the reporter construct. The *ZmbZIP89* CDS was cloned into the pGreenII 62-SK vector to generate the effector construct. The recombinant vectors were transferred into *A. tumefaciens* strain GV3101 (pSoup-P19) cells for the cotransformation of the leaves of 4-week-old *N. benthamiana* plants. Three days later, the infiltrated areas of leaves were collected, and proteins were extracted. Relative LUC activities were measured using the a Dual-Luciferase Reporter Assay System kit (E1910, Promega).

Y1H assay

Two *ZmPRX47* promoter fragments (−476 to −322 bp and −322 to −212 bp) were cloned into separate pBait-AbAi vectors, with the resulting recombinant vectors (pBait-pAbAi-1 and pBait-pAbAi-2, respectively) inserted into Y1H Gold yeast strain cells according to the manufacturer's instructions (Clontech Laboratories Inc., San Jose, CA, USA). The growth of the cotransformed cells on solid culture medium supplemented with varying concentrations of aureobasidin A (AbA) (SD/−Ura/0, 100, 200, 300, 500, 700, and 900 ng/ml) was assessed. We selected the AbA concentration that inhibited growth for subsequent experiments. The *ZmbZIP89* CDS was cloned into the pGADT7 vector to produce the prey construct. After ruling out self-activation, the recombinant vectors were transformed into Y1H Gold yeast strain cells as described by the manufacturer (Clontech Laboratories Inc.). The growth of the cotransformed cells on solid culture media [SD/−Leu and SD/−Leu/AbA (500 ng/ml)] was examined. Primer pairs are listed in table S15.

Electrophoretic mobility shift assay

The *ZmbZIP89* CDS was inserted into the pCold-TF vector for the expression of the His-ZmbZIP89 recombinant protein in *Escherichia coli* BL21 cells. To obtain soluble His-ZmbZIP89 proteins, *E. coli* cells harboring the pCold-TF-His-ZmbZIP89 recombinant vector were cultured at 16°C for 24 hours, with protein expression induced by the addition of 1 mM isopropyl-β-D-thiogalactopyranoside. Recombinant His-ZmbZIP89 was isolated from *E. coli* cells and purified using Ni-NTA His Bind Resin. A labeled double-stranded probe was amplified directly using a standard PCR method and then added to annealing buffer to form a double-stranded probe, which was purified using a DNA purification kit and eluted with 100 to 200 μl of water. An unlabeled probe was added as a competitor to the reaction solutions, which were incubated at room temperature for 30 min. Samples were separated by electrophoresis using native polyacrylamide gels (8% acrylamide and bis-acrylamide, 39:1). Fluorescent gel images were obtained using an Amersham Typhoon system.

ZmbZIP89-based association analysis

After excluding 121 progenies from CUBIC, we randomly selected 164 inbred lines from 236 inbred lines for a candidate gene association analysis (table S1). Genomic DNA was extracted from young leaves and sequenced using the DNBSEQ-T7 platform (>10 × per genome). Raw reads were pre-processed using Trim Galore (v0.6.10) to remove low-quality bases and adapters. High-quality reads were mapped to the Zm-B73-REFERENCE-NAM-5.0 using Burrow-Wheeler Aligner (BWA) (v0.7.17-r1188), with BAM files sorted and indexed using SAMtools (v1.6). SNPs were identified using GATK (v4.2.6.1). For each sample, GVCFs were generated using HaplotypeCaller, and then CombineGVCFs and GenotypeGVCFs were used to produce a VCF file. Variants were further filtered using VariantFiltration. SNPs and InDels in the 2000-bp promoter, 784-bp 5′ UTR, 1298-bp coding regions (including introns), and 414-bp 3′UTR of *ZmbZIP89* were extracted and filtered by minor allele frequency (MAF) ≥ 0.05. Associations between SNPs and *ZmbZIP89* expression as well as LRL were calculated by TASSEL (v5.2.92), under the standard mixed linear model (MLM). The SNP data for analyzing the allele frequencies of SNP1400 and SNP1419 in *ZmbZIP89* in teosinte and maize germplasm were downloaded from an online database https://ftp.cngb.org/pub/CNSA/data3/CNP0001565/zeamap/02_Variants/PAN_Zea_Variants/Zea-vardb/ (*24*). In addition, 15 lines per haplotype (table S1) were grown in a cultivation box system as described above under well-watered and drought conditions to assess their drought resilience.

Transient *LUC* expression assays

To investigate whether variants in 3′UTR affect *ZmbZIP89* mRNA abundance, the 434- and 415-bp Hap1 and Hap2 *ZmbZIP89* 3′UTR sequences were amplified, respectively. Each amplified fragment was inserted downstream of the *LUC* CDS in the pGreenII 0800 miRNA-LUC vector. The recombinant vectors were transferred into *A. tumefaciens* strain GV3101 (pSoup-P19) cells. *A. tumefaciens* cells harboring the reporter and effector constructs were used for the transformation of leaves from 4-week-old *N. benthamiana* plants. Three days later, the infiltrated areas of leaves were collected, and proteins were extracted. LUC activity was measured using the Dual-Luciferase Reporter Assay System Kit (E1910, Promega). Four biological replicates, each with three technical replicates, were assayed per vector.

mRNA stability assay

To assess mRNA stability in *N. benthamiana* leaves, the *ZmbZIP89* CDS was amplified from B73 cDNA. The Hap1 and Hap2 *ZmbZIP89* 3′UTR sequences were amplified and individually fused downstream of the $ZmbZIP89^{B73}$ CDS. The generated fusion constructs were cloned into the pGreenII 62-SK vector and then transformed into *A. tumefaciens* strain GV3101 (pSoup) cells. Transformed *A. tumefaciens* cells were cultured at 28°C for 18 hours in LB liquid medium containing kanamycin (50 μg ml^{-1}), gentamycin (50 μg ml^{-1}), and rifampicin (50 μg ml^{-1}). The cell culture was centrifuged at 5000*g* for 5 min, and then the pelleted *A. tumefaciens* cells were resuspended in infiltration buffer [10 mM MES (pH 5.6), 10 mM $MgCl_2$, and 100 μM acetosyringone] for an optical density at 600 of 0.5 before the infiltration of *N. benthamiana* leaves. After a 36-hour incubation, the infiltrated parts of leaves were injected with actinomycin D (20 μg ml^{-1}; MCE, HY-17559). After culturing for 15 min, leaf discs were collected and used as the time zero (t0) control. Additional leaf discs were collected in triplicate every 90 min.

To evaluate mRNA stability in maize, roots from 14-day-old seedlings of Hap1 and Hap2 inbred lines were sliced into 3-cm segments and incubated in sterile water containing actinomycin D (20 μg ml^{-1}). After a 30-min incubation, root segments were collected as time zero (t0) control samples. Additional root samples were collected in triplicate every 3 hours. The mRNA levels of selected genes were subsequently examined by quantitative RT-PCR.

Statistical analysis

Pairwise differences between genotypes were assessed using a two-tailed Student's *t* test. For comparisons involving more than two genotypes, statistical analyses were conducted using one-way analysis of variance followed by Tukey's post hoc test.

Supplementary Materials

The PDF file includes:

Figs. S1 to S26

Legends for tables S1 to S15

Other Supplementary Material for this manuscript includes the following:

Tables S1 to S15

REFERENCES AND NOTES

1. F. Hochholdinger, P. Yu, C. Marcon, Genetic control of root system development in maize. *Trends Plant Sci.* **23**, 79–88 (2018).
2. P. Yu, J. A. Baldauf, A. Lithio, C. Marcon, D. Nettleton, C. Li, F. Hochholdinger, Root type-specific reprogramming of maize pericycle transcriptomes by local high nitrate results in disparate lateral root branching patterns. *Plant Physiol.* **170**, 1783–1798 (2016).
3. Z. Jia, R. F. H. Giehl, N. von Wirén, Local auxin biosynthesis acts downstream of brassinosteroids to trigger root foraging for nitrogen. *Nat. Commun.* **12**, 5437 (2021).
4. V. Protto, F. Bauget, L. Rishmawi, P. Nacry, C. Maurel, Primary, seminal and lateral roots of maize show type-specific growth and hydraulic responses to water deficit. *Plant Physiol.* **194**, 2564–2579 (2024).
5. C. Maurel, P. Nacry, Root architecture and hydraulics converge for acclimation to changing water availability. *Nat. Plants* **6**, 744–749 (2020).
6. P. Yu, F. Hochholdinger, C. Li, Plasticity of lateral root branching in maize. *Front. Plant Sci.* **10**, 363 (2019).
7. I. Lopez-Valdivia, A. C. Perkins, H. M. Schneider, M. Vallebueno-Estrada, J. D. Burridge, E. González-Orozco, A. Montufar, R. Montiel, J. P. Lynch, J.-P. Vielle-Calzada, Gradual domestication of root traits in the earliest maize from Tehuacán. *Proc. Natl. Acad. Sci. U.S.A.* **119**, e2110245119 (2022).
8. P. Yu, C. Li, M. Li, X. He, D. Wang, H. Li, C. Marcon, Y. Li, S. Perez-Limón, X. Chen, M. Delgado-Baquerizo, R. Koller, R. Metzner, D. van Dusschoten, D. Pflugfelder, L. Borisjuk, I. Plutenko, A. Mahon, M. F. R. Resende Jr., S. Salvi, A. Akale, M. Abdalla, M. A. Ahmed, F. M. Bauer, A. Schnepf, G. Lobet, A. Heymans, K. Suresh, L. Schreiber, C. M. McLaughlin, C. Li, M. Mayer, C.-C. Schön, V. Bernau, N. von Wirén, R. J. H. Sawers, T. Wang, F. Hochholdinger, Seedling root system adaptation to water availability during maize domestication and global expansion. *Nat. Genet.* **56**, 1245–1256 (2024).
9. Y. Uga, K. Sugimoto, S. Ogawa, J. Rane, M. Ishitani, N. Hara, Y. Kitomi, Y. Inukai, K. Ono, N. Kanno, H. Inoue, H. Takehisa, R. Motoyama, Y. Nagamura, J. Wu, T. Matsumoto, T. Takai, K. Okuno, M. Yano, Control of root system architecture by *DEEPER ROOTING 1* increases rice yield under drought conditions. *Nat. Genet.* **45**, 1097–1102 (2013).
10. M. Zhang, Y. Chen, H. Xing, W. Ke, Y. Shi, Z. Sui, R. Xu, L. Gao, G. Guo, J. Li, J. Xing, Y. Zhang, Positional cloning and characterization reveal the role of a miRNA precursor gene *ZmLRT* in the regulation of lateral root number and drought tolerance in maize. *J. Integr. Plant Biol.* **65**, 772–790 (2022).
11. X. Feng, J. Xiong, W. Zhang, H. Guan, D. Zheng, H. Xiong, L. Jia, Y. Hu, H. Zhou, Y. Wen, X. Zhang, F. Wu, Q. Wang, J. Xu, Y. Lu, ZmLBD5, a class-II LBD gene, negatively regulates drought tolerance by impairing abscisic acid synthesis. *Plant J.* **112**, 1364–1376 (2022).
12. H. Ma, C. Liu, Z. Li, Q. Ran, G. Xie, B. Wang, S. Fang, J. Chu, J. Zhang, ZmbZIP4 contributes to stress resistance in maize by regulating ABA synthesis and root development. *Plant Physiol.* **178**, 753–770 (2018).
13. P. Yu, C. Gutjahr, C. Li, F. Hochholdinger, Genetic control of lateral root formation in cereals. *Trends Plant Sci.* **21**, 951–961 (2016).
14. J. A. Santos Teixeira, K. H. ten Tusscher, The systems biology of lateral root formation: Connecting the dots. *Mol. Plant* **12**, 784–803 (2019).
15. A. Vilches-Barro, A. Maizel, Talking through walls: Mechanisms of lateral root emergence in *Arabidopsis thaliana*. *Curr. Opin. Plant Biol.* **23**, 31–38 (2015).
16. P. Yu, F. Hochholdinger, C. Li, Root-type-specific plasticity in response to localized high nitrate supply in maize (*Zea mays*). *Ann. Bot.* **116**, 751–762 (2015).
17. C. Ortiz-Ramirez, B. Guillotin, X. Xu, R. Rahni, S. Zhang, Z. Yan, P. Coqueiro Dias Araujo, E. Demesa-Arevalo, L. Lee, J. Van Eck, T. R. Gingeras, D. Jackson, K. L. Gallagher, K. D. Birnbaum, Ground tissue circuitry regulates organ complexity in maize and *Setaria*. *Science* **374**, 1247–1252 (2021).
18. T. M. Nolan, N. Vukasinovic, C. W. Hsu, J. Zhang, I. Vanhoutte, R. Shahan, I. W. Taylor, L. Greenstreet, M. Heitz, A. Afanassiev, P. Wang, P. Szekely, A. Brosnan, Y. Yin, G. Schiebinger, U. Ohler, E. Russinova, P. N. Benfey, Brassinosteroid gene regulatory networks at cellular resolution in the *Arabidopsis* root. *Science* **379**, eadf4721 (2023).
19. J. R. Wendrich, B. J. Yang, N. Vandamme, K. Verstaen, W. Smet, C. Van de Velde, M. Minne, B. Wybouw, E. Mor, H. E. Arents, J. Nolf, J. Van Duyse, G. Van Isterdael, S. Maere, Y. Saeys, B. De Rybel, Vascular transcription factors guide plant epidermal responses to limiting phosphate conditions. *Science* **370**, eaay4970 (2020).
20. Q. Liu, Z. Liang, D. Feng, S. Jiang, Y. Wang, Z. Du, R. Li, G. Hu, P. Zhang, Y. Ma, J. U. Lohmann, X. Gu, Transcriptional landscape of rice roots at the single-cell resolution. *Mol. Plant* **14**, 384–394 (2021).
21. Y. Hacham, N. Holland, C. Butterfield, S. Ubeda-Tomas, M. J. Bennett, J. Chory, S. Savaldi-Goldstein, Brassinosteroid perception in the epidermis controls root meristem size. *Development* **138**, 839–848 (2011).
22. O. Contreras-López, E. A. Vidal, E. Riveras, J. M. Alvarez, T. C. Moyano, E. E. Sparks, J. Medina, A. Pasquino, P. N. Benfey, G. M. Coruzzi, R. A. Gutiérrez, Spatiotemporal analysis identifies ABF2 and ABF3 as key hubs of endodermal response to nitrate. *Proc. Natl. Acad. Sci. U.S.A.* **119**, e2107879119 (2022).
23. S. Aibar, C. B. González-Blas, T. Moerman, V. A. Huynh-Thu, H. Imrichova, G. Hulselmans, F. Rambow, J.-C. Marine, P. Geurts, J. Aerts, J. van den Oord, Z. K. Atak, J. Wouters, S. Aerts, SCENIC: Single-cell regulatory network inference and clustering. *Nat. Methods* **14**, 1083–1086 (2017).
24. L. Chen, J. Luo, M. Jin, N. Yang, X. Liu, Y. Peng, W. Li, A. Phillips, B. Cameron, J. S. Bernal, R. Rellán-Álvarez, R. J. H. Sawers, Q. Liu, Y. Yin, X. Ye, J. Yan, Q. Zhang, X. Zhang, S. Wu, S. Gui, W. Wei, Y. Wang, Y. Luo, C. Jiang, M. Deng, M. Jin, L. Jian, Y. Yu, M. Zhang, X. Yang, M. B. Hufford, A. R. Fernie, M. L. Warburton, J. Ross-Ibarra, J. Yan, Genome sequencing reveals evidence of adaptive variation in the genus. *Nat. Genet.* **54**, 1736–1745 (2022).
25. P. Voothuluru, Y. Wu, R. E. Sharp, Not so hidden anymore: Advances and challenges in understanding root growth under water deficits. *Plant Cell* **36**, 1377–1409 (2024).
26. D. F. Placido, J. Sandhu, S. J. Sato, N. Nersesian, T. Quach, T. E. Clemente, P. E. Staswick, H. Walia, The *LATERAL ROOT DENSITY* gene regulates root growth during water stress in wheat. *Plant Biotechnol. J.* **18**, 1955–1968 (2020).
27. J. Gao, Y. Zhao, Z. Zhao, W. Liu, C. Jiang, J. Li, Z. Zhang, H. Zhang, Y. Zhang, X. Wang, X. Sun, Z. Li, RRS1 shapes robust root system to enhance drought resistance in rice. *New Phytol.* **238**, 1146–1162 (2023).
28. X. Wang, H. Wang, S. Liu, A. Ferjani, J. Li, J. Yan, X. Yang, F. Qin, Genetic variation in *ZmVPP1* contributes to drought tolerance in maize seedlings. *Nat. Genet.* **48**, 1233–1241 (2016).
29. M. Baer, G. Taramino, D. Multani, H. Sakai, S. Jiao, K. Fengler, F. Hochholdinger, Maize *lateral rootless 1* encodes a homolog of the DCAF protein subunit of the CUL4-based E3 ubiquitin ligase complex. *New Phytol.* **237**, 1204–1214 (2022).
30. I. von Behrens, M. Komatsu, Y. Zhang, K. W. Berendzen, X. Niu, H. Sakai, G. Taramino, F. Hochholdinger, Rootless with undetectable meristem 1 encodes a monocot-specific AUX/IAA protein that controls embryonic seminal and post-embryonic lateral root initiation in maize. *Plant J.* **66**, 341–353 (2011).
31. C. Zheng, X. Wang, Y. Xu, S. Wang, X. Jiang, X. Liu, W. Cui, Y. Wu, C. Yan, H. Liu, Y. Lu, J. Chen, J. Zhou, The peroxidase gene OsPrx114 activated by OsWRKY50 enhances drought tolerance through ROS scavenging in rice. *Plant Physiol. Biochem.* **204**, 108138 (2023).
32. Z. Zhang, J. Ma, X. Yang, Z. Liu, Y. Liu, X. Liu, S. Liang, Z. Duan, Z. Wang, X. Yang, L. Yan, M. Zhang, S. Liu, Z. Tian, Natural allelic diversities of *GmPrx16* confer drought tolerance in soybean. *Plant Biotechnol. J.* **22**, 535–537 (2023).
33. Y. Zhang, X. Wu, X. Wang, M. Dai, Y. Peng, Crop root system architecture in drought response. *J. Genet. Genomics* **52**, 4–13 (2025).
34. D. van Dusschoten, J. Kochs, C. W. Kuppe, V. A. Sydoruk, V. Couvreur, D. Pflugfelder, J. A. Postma, Spatially resolved root water uptake determination using a precise soil water sensor. *Plant Physiol.* **184**, 1221–1235 (2020).
35. H. Tsukagoshi, Control of root growth and development by reactive oxygen species. *Curr. Opin. Plant Biol.* **29**, 57–63 (2016).
36. P. Li, X. Yang, H. Wang, T. Pan, Y. Wang, Y. Xu, C. Xu, Z. Yang, Genetic control of root plasticity in response to salt stress in maize. *Theor. Appl. Genet.* **134**, 1475–1492 (2021).
37. H.-J. Liu, X. Wang, Y. Xiao, J. Luo, F. Qiao, W. Yang, R. Zhang, Y. Meng, J. Sun, S. Yan, Y. Peng, L. Niu, L. Jian, W. Song, J. Yan, C. Li, Y. Zhao, Y. Liu, M. L. Warburton, J. Zhao, J. Yan, CUBIC: An atlas of genetic architecture promises directed maize improvement. *Genome Biol.* **21**, 20 (2020).
38. L. Ming, D. Fu, Z. Wu, H. Zhao, X. Xu, T. Xu, X. Xiong, M. Li, Y. Zheng, G. Li, L. Yang, C. Xia, R. Zhou, K. Liao, Q. Yu, W. Chai, S. Li, Y. Liu, X. Wu, J. Mao, J. Wei, X. Li, L. Wang, C. Wu, W. Xie, Transcriptome-wide association analyses reveal the impact of regulatory variants on rice panicle architecture and causal gene regulatory networks. *Nat. Commun.* **14**, 7501 (2023).
39. S. Liu, C. Li, H. Wang, S. Wang, S. Yang, X. Liu, J. Yan, B. Li, M. Beatty, G. Zastrow-Hayes, S. Song, F. Qin, Mapping regulatory variants controlling gene expression in drought response and tolerance in maize. *Genome Biol.* **21**, 163 (2020).
40. H. M. Kang, J. H. Sul, S. K. Services, N. A. Zaitlen, S.-y. Kong, N. B. Freimer, C. Sabatti, E. Eskin, Variance component model to account for sample structure in genome-wide association studies. *Nat. Genet.* **42**, 348–354 (2010).
41. S.-D. Yoo, Y.-H. Cho, J. Sheen, Arabidopsis mesophyll protoplasts: A versatile cell system for transient gene expression analysis. *Nat. Protoc.* **2**, 1565–1572 (2007).
42. Y. Hao, S. Hao, E. Andersen-Nissen, W. M. Mauck III, S. Zheng, A. Butler, M. J. Lee, A. J. Wilk, C. Darby, M. Zager, P. Hoffman, M. Stoeckius, E. Papalexi, E. P. Mimitou, J. Jain, A. Srivastava, T. Stuart, L. M. Fleming, B. Yeung, A. J. Rogers, J. M. McElrath, C. A. Blish, R. Gottardo, P. Smibert, R. Satija, Integrated analysis of multimodal single-cell data. *Cell* **184**, 3573–3587.e29 (2021).
43. J. Cheng, G. K. Smyth, Y. Chen, Unraveling the timeline of gene expression: A pseudotemporal trajectory analysis of single-cell RNA sequencing data. *F1000Res.* **12**, 684 (2023).
44. E. Becht, L. McInnes, J. Healy, C.-A. Dutertre, I. W. H. Kwok, L. G. Ng, F. Ginhoux, E. W. Newell, Dimensionality reduction for visualizing single-cell data using UMAP. *Nat. Biotechnol.* **37**, 38–44 (2018).
45. A. P. Marand, Z. Chen, A. Gallavotti, R. J. Schmitz, A cis-regulatory atlas in maize at single-cell resolution. *Cell* **184**, 3041–3055.e21 (2021).

46. X. Li, X. Zhang, S. Gao, F. Cui, W. Chen, L. Fan, Y. Qi, Single-cell RNA sequencing reveals the landscape of maize root tips and assists in identification of cell type-specific nitrate-response genes. *Crop J.* **10**, 1589–1600 (2022).
47. X. Qiu, A. Hill, J. Packer, D. Lin, Y.-A. Ma, C. Trapnell, Single-cell mRNA quantification and differential analysis with Census. *Nat. Methods* **14**, 309–315 (2017).
48. V. Bergen, M. Lange, S. Peidli, F. A. Wolf, F. J. Theis, Generalizing RNA velocity to transient cell states through dynamical modeling. *Nat. Biotechnol.* **38**, 1408–1414 (2020).
49. A. M. Newman, C. B. Steen, C. L. Liu, A. J. Gentles, A. A. Chaudhuri, F. Scherer, M. S. Khodadoust, M. S. Esfahani, B. A. Luca, D. Steiner, M. Diehn, A. A. Alizadeh, Determining cell type abundance and expression from bulk tissues with digital cytometry. *Nat. Biotechnol.* **37**, 773–782 (2019).
50. A. Bartlett, R. C. O'Malley, S.-s. C. Huang, M. Galli, J. R. Nery, A. Gallavotti, J. R. Ecker, Mapping genome-wide transcription-factor binding sites using DAP-seq. *Nat. Protoc.* **12**, 1659–1672 (2017).
51. T. Chen, C. Guestrin, paper presented at the 22nd ACM SIGKDD International Conference on Knowledge Discovery and Data Mining, San Francisco, California, USA, 13 to 17 August 2016.
52. S. Chen, P. Songkumarn, J. Liu, G.-L. Wang, A versatile zero background T-vector system for gene cloning and functional genomics. *Plant Physiol.* **150**, 1111–1121 (2009).
53. Y. Ishida, Y. Hiei, T. Komari, *Agrobacterium*-mediated transformation of maize. *Nat. Protoc.* **2**, 1614–1621 (2007).

Acknowledgments: We thank J. Yan (Huazhong Agricultural University) for sharing the CUBIC population. **Funding:** This work was supported by the National Key Technology Research and Development Program of Ministry of Science and Technology of China (2022YFD1900704 to P.L. and 2022YFD1201804 to C.X.), the National Natural Science Foundation of China (32302654 to Y.W., 31972487 to P.L., 32172009 to C.X., and 32061143030 to C.X.), the Jiangsu Province University Basic Science Research Project (21KJA210002 to P.L.), the Open Research Fund Program of State Key Laboratory of Nutrient Use and Management (KF2024-9 to P.L.), the Innovative Research Team of Universities in Jiangsu Province, the High-end Talent Project of Yangzhou University (to P.L.), the Priority Academic Program Development of Jiangsu Higher Education Institutions (PAPD), and the Qing Lan Project of Jiangsu Province (to P.L.). **Author contributions:** Conceptualization: C.X., P.Y., and P.L. Investigation: C.X., Y.W., P.Y., Y.D., H.W., X.Y., T.Z., X.Z., W.R., A.Y., Y.Y., W.L., P.L., and S.F. Writing (review and editing): C.X., Y.W., Z.Y., P.Y., Y.D., H.W., X.Y., T.Z., X.Z., W.R., Z.J., A.Y., Y. Y, W.L., Q.P., P.L., and S.F. Writing (original draft): P.Y., T.Z., and P.L. Methodology: C.X., P.Y., and P.L. Resources: C.X., Y.W., Y.D., X.Y., T.Z., W.R., A.Y., Y.Y., W.L., P.L., and S.F. Funding acquisition: C.X., Y.W., and P.L. Data curation: C.X., Y.W., Z.Y., P.Y., T.Z., and P.L. Validation: C.X., Y.W., P.Y., T.Z., P.L., and S.F. Project administration: C.X., P.Y., and P.L. Formal analysis: Z.Y., P.Y., T.Z., and P.L. Software: P.Y., T.Z., and P.L. Visualization: P.Y., T.Z., and P.L. Supervision: P.L. **Competing interests:** The authors declare that they have no competing interests. **Data and materials availability:** All data needed to evaluate the conclusions in this paper are present in the paper and/or the Supplementary Materials. The bulk RNA-seq reads from this study were deposited in the NCBI Sequence Read Archive (www.ncbi.nlm.nih.gov/sra) with the accession codes SRP446501/PRJNA980895. The scRNA-seq, DAP-seq, and DNA sequencing source data are deposited in the Genome Sequence Archive (https://bigd.big.ac.cn/gsa) under accession number CRA018050, CRA018051, and CRA017878. The codes used in this article can be accessed at https://doi.org/10.5061/dryad.nzs7h451h.

Submitted 12 September 2024
Accepted 7 March 2025
Published 11 April 2025
10.1126/sciadv.adt1113